



#### **OPEN ACCESS**

EDITED BY Amit Sharma,

North Carolina State University, United States

REVIEWED BY

Diako Ebrahimi, Texas Biomedical Research Institute, United States Chen Liang, McGill University, Canada

\*CORRESPONDENCE

RECEIVED 14 June 2025 ACCEPTED 04 August 2025 PUBLISHED 21 August 2025

#### CITATION

Prikryl D, Zhang Y, Verma S and Melikyan GB (2025) Attenuation of IFITM proteins' antiviral activity through sequestration into intraluminal vesicles of late endosomes. *Front. Immunol.* 16:1647166. doi: 10.3389/fimmu.2025.1647166

#### COPYRIGHT

© 2025 Prikryl, Zhang, Verma and Melikyan. This is an open-access article distributed under the terms of the Creative Commons Attribution License (CC BY). The use, distribution or reproduction in other forums is permitted, provided the original author(s) and the copyright owner(s) are credited and that the original publication in this journal is cited, in accordance with accepted academic practice. No use, distribution or reproduction is permitted which does not comply with these terms.

# Attenuation of IFITM proteins' antiviral activity through sequestration into intraluminal vesicles of late endosomes

David Prikryl<sup>1</sup>, You Zhang<sup>1</sup>, Smita Verma<sup>1</sup> and Gregory B. Melikyan<sup>1,2\*</sup>

<sup>1</sup>Department of Pediatrics, Division of Infectious Diseases, Emory University School of Medicine, Atlanta, GA, United States, <sup>2</sup>Children's Healthcare of Atlanta, Atlanta, GA, United States

**Introduction:** Interferon-induced transmembrane proteins (IFITMs) inhibit the entry of diverse enveloped viruses. The spectrum of antiviral activity of IFITMs is largely determined by their subcellular localization. IFITM1 localizes to and primarily blocks viral fusion at the plasma membrane, while IFITM3 prevents viral fusion in late endosomes by accumulating in these compartments. We and others have previously shown that cyclosporine treatment relieves the fusion block for the Influenza A virus, but the mechanism of this rescue remained unclear.

**Results:** Here, we report the existence of at least two distinct pools of IFITMs in cyclosporine treated cells. Major pools of IFITM1 and IFITM3 were found in endosomes, with IFITM1 relocating from the plasma membrane by a mechanism involving macropinocytosis, while the newly synthesized IFITMs were trapped in the Golgi. We noted that cyclosporine-mediated IFITM redistribution to late endosomes was not associated with its degradation. Importantly, cyclosporine treatment restricted antibody access to the cytoplasmic N-terminus but not to the extracellular C-terminus of IFITMs, consistent with IFITM sequestration in intraluminal vesicles of late endosomes. Indeed, super-resolution microscopy revealed that cyclosporine induces IFITM3 redistribution from the periphery to the interior of late endosomes.

**Discussion:** Together, our results imply that IFITMs relocate to intraluminal vesicles of late endosomes in the presence of cyclosporine, thereby enabling viral fusion with the limiting membrane of these compartments. Our findings highlight the critical role of IFITM trafficking in antiviral defense and suggest a novel mechanism through which cyclosporine modulates the cell's susceptibility to viral infections.

#### KEYWORDS

IFITM, cyclosporine A, virus restriction, viral fusion, super-resolution microscopy, endocytosis, intraluminal vesicles, membrane permeabilization

#### 1 Introduction

Interferon-induced transmembrane proteins (IFITMs) impose a barrier to fusion of diverse enveloped viruses, such as the Influenza A Virus (IAV), Vesicular Stomatitis Virus (VSV), Respiratory syncytial virus (RSV), Dengue Virus, Ebola Virus, Measles Virus and other pathogenic viruses. Notable exceptions include the Murine Leukemia Virus and arenaviruses, such as the Lassa Virus (LASV), which are insensitive to IFITM restriction (1-4). The human genome encodes for five IFITM proteins, with IFITM1, IFITM2, and IFITM3 exhibiting antiviral activity (5-7). The significance of IFITM-mediated virus restriction in vivo is underscored by studies demonstrating that Ifitm3 knockout mice succumb to IAV or RSV infection (8-11). Additionally, several groups have established a correlation between single-nucleotide polymorphisms (SNPs) in the Ifitm3 gene and more severe outcomes of IAV or severe acute respiratory syndrome coronavirus 2 (SARS-CoV-2) infection (12-16).

The range of restricted viruses is largely determined by the subcellular localization of IFITMs, which is regulated predominantly by the YXXL endocytic sorting motif within the N-terminal domain of IFITM2 and IFITM3. This motif is recognized by the clathrin adaptor protein 2 (AP2), which drives their internalization and concentration in endosomes, effectively preventing viruses from entering cells through an endocytic route (17–20). Conversely, IFITM1 lacking the N-terminal endocytic signal predominantly resides in the plasma membrane (PM) and is more efficacious against viruses that tend to fuse at this location (2, 5, 21, 22).

The IFITMs' antiviral activity is further modulated through various post-translational modifications, including Spalmitoylation, ubiquitylation, phosphorylation, and methylation (23-28). Subcellular localization and antiviral activity of IFITMs can also be altered by treatment with certain compounds, as reported by us and other groups (29-32). However, the results on changes in the subcellular localization of IFITM3 in treated cells differ between groups. We have found that cyclosporine A (CsA) triggered a rapid relocalization of IFITMs to the Golgi area without a noticeable degradation of these proteins. In contrast, others reported a strong colocalization of IFITM3 with the endolysosomal compartments that promote degradation after prolonged treatment with either rapamycin or cyclosporine H (29-31). However, the mechanism by which cyclosporines modulate the localization and abundance of IFITMs remains unclear.

Here, to address the above discrepancies regarding the mechanism of cyclosporine antagonism with IFITMs' function, we carried out comprehensive studies of CsA-driven IFITMs relocalization under varying conditions and correlated them with rescue of IAV fusion. Our results imply that CsA redirects IFITM1 and IFITM3 from the PM and the limiting membrane of endosomes, respectively, to the intraluminal vesicles (ILVs) of late endosomes. Such massive relocalization is not detectable in mildly permeabilized cells due to poor ILV accessibility to antibodies. We confirmed the CsA-induced IFITM3 redistribution to ILVs by

super-resolution microscopy. These findings reconcile the reported differences in protein distribution and abundance and provide a plausible mechanism of CsA-mediated rescue of viral fusion in IFITM-expressing cells. This mechanism involves an effective removal of IFITMs from the PM and the limiting membrane of late endosomes, where productive viral fusion takes place.

#### 2 Materials and methods

#### 2.1 Cell lines, reagents, and plasmids

Human A549, HEK293T/17, and HeLa cells were obtained from ATCC (Manassas, VA, USA) and grown in Dulbecco's Modified Eagle Medium (DMEM) supplemented with 10% heat-inactivated fetal bovine serum (FBS, Atlanta Biologicals, Flowery Branch, GA, USA), 100 U penicillin-streptomycin (Gemini Bio-Products, Sacramento, CA, USA). Stable cell lines A549.vector, A549.IFITM1-FLAG, A549.FLAG-IFITM1, A549.IFITM3, and A549.IFITM3-iSNAP ectopically expressing the respective IFITM proteins have been described previously (33, 34). Briefly, cells were transduced with VSV-G-pseudotyped viruses encoding wild-type or flag-tagged IFITMs or with the empty vector, pQCXIP (Takara, Shiga, Japan), and selected with 1.5 μg/mL puromycin.

Bafilomycin A1 (Cat. B1793), NH<sub>4</sub>Cl (Cat. A0171), E64d (Cat. E8640), Cyclosporine A (Cat. 30024), cycloheximide (Cat. C7698), rapamycin (Cat. 553210), Triton X-100, Streptolysin O, melittin, and acetone were from Sigma (St. Louis, MO, USA). MG-132 (Cat. 474791) was purchased from Calbiochem (Columbus, OH, USA). Lactacystin (sc-3575) was purchased from Santa Cruz Biotech (Dallas, TX, USA). Recombinant human EGF (Cat. 236-EG) was purchased from R&D Systems (Minneapolis, MN, USA). Nonidet P-40 was purchased from USBiological (Salem, MA, USA), Tween 20 was obtained from J.T. Baker (Phillipsburg, NJ, USA), methanol was from Fisher Chemicals (Zurich, Switzerland), and Digitonin was purchased from Invitrogen (Cat. 11024-24-1, Research product international, Mount Prospect, Illinois). MK-2206 was from Selleckchem (Cat. S1078, Houston, TX). SNAP-Cell 647-SiR (Cat. S9102S) and SNAP-Cell Oregon Green (Cat. S9104S) were purchased from New England Biolabs (Ipswich, MA, USA). FM1-43 dye (Cat. T35356) and Alexa Fluor 568 (AF568) NHS Ester (Cat. A20103) were purchased from Invitrogen (Waltham, MA, USA). mCLING labeled with ATTO 647N (Cat. 710 006AT647N) was obtained from Synaptic Systems (Goettingen, Germany). The Influenza A/PR/8/34 virus (Cat. 10100374) was purchased from Charles River Laboratories (Wilmington, MA, USA).

Antibodies used were rabbit anti-IFITM3 (Abcam, Cambridge, UK), mouse anti-IFITM2/3 (Proteintech, San Diego, CA, USA), rabbit anti-IFITM1 (Sigma), mouse anti-GM130 (BD Bioscience, Franklin Lakes, NJ, USA), sheep anti-TGN46 (Bio-Rad AbD Serotec Limited, Luxembourg), mouse anti-Rab6A, clone 5B10 (a gift from Prof. Angelika Barnekow, Münster University, Germany), mouse anti-flag<sup>®</sup> M2 (Sigma), mouse anti-Human CD63 (BD Biosciences), Influenza A NP recombinant rabbit monoclonal antibody (Fisher)

and antibody to the EGFR N-terminus (Calbiochem), antibody to the EGFR C-terminus (Cell Signaling, Danvers, MA, USA), AF568 Goat anti-Mouse IgG (H+L) (Invitrogen, Waltham, MA, USA), Goat anti-rabbit IgG (H+L) conjugated with AF647 (ThermoFisher, Waltham, MA, USA), and Donkey anti-sheep IgG (H+L) conjugated with AF568 (Abcam). Secondary antibodies conjugated with STED-compatible dyes were STAR RED (STRED-1002) and STAR 580 (ST580-1001), both purchased from Abberior, Germany.

The pCAGGS vectors encoding influenza H1N1 WSN HA and NA were kindly provided by Donna Tscherne and Peter Palese (Icahn School of Medicine, Mount Sinai). The eGFP-Vpr plasmid was a gift from T. Hope (Northwestern University). The HIV-1 packaging vector pR9ΔEnvΔNef and pcRev have been described previously (35). The pQCXIP vector-based constructs encoding human IFITM1 and IFITM3 were generously provided by Dr. A.L. Brass (1).

#### 2.2 Pseudovirus production

Pseudovirus production and plasmid details were previously described (32, 35). Briefly, HEK293T/17 cells were transfected using JetPRIME. For IAV pseudoviruses (IAVpp), cells in 100-mm dishes were transfected with pR9 $\Delta$ Env (5 µg), MM310 plasmid encoding Vpr fused to  $\beta$ -lactamase (1.5 µg), pcRev (1 µg), and pCAGGS-WSN HA/NA (2.5 µg each). For LASV pseudoviruses (LASVpp), 4 µg of Lassa GPC plasmid replaced HA/NA. After 12 h, the medium was replaced with phenol red-free media; supernatants were collected 36 h later, filtered (0.45 µm), concentrated 10× (Lenti-X), and aliquots stored at  $-80^{\circ}$ C.

For infectivity assays, IAVpp were made in 6-well plates using similar transfection conditions: pR9 $\Delta$ Env $\Delta$ Nef (0.8 µg), eGFP-Vpr (0.14 µg), pcRev (0.2 µg), pCAGGS-WSN HA/NA (0.3 µg each), and either IFITM1, IFITM3, or control vector (0.3 µg). GFP-Vpr was included to visualize single virions for another study. Supernatants were collected, as above, resuspended in PBS, aliquoted and stored at -80°C. The p24 content of pseudoviruses was determined by ELISA assay, as previously described (36).

## 2.3 IAV labeling, purification, and characterization

Twenty-five  $\mu L$  of freshly prepared 1 M sodium bicarbonate (pH 9.0) buffer was mixed with 75  $\mu L$  of ultrapure water to make the reaction solution. Fifty  $\mu L$  of IAV (2 mg/mL of total protein) was mixed with 100  $\mu L$  of reaction solution and incubated for 1 hour at room temperature with AF568-NHS at a concentration of 50  $\mu M$  by agitating in the dark at the lowest speed of a vortex. After incubation, NHS activity was quenched by adding 3  $\mu L$  of 1 M Tris-buffer (pH 8.0). Unbound dye was removed using NAP-5 gel filtration column (Illustra, Danaher Corporation, USA) according to the manufacture's manual. Labeled IAV was eluted with 500  $\mu L$  of PBS without calcium and magnesium (PBS  $^{-/-}$ ; 21-040-CV,

Corning), and filtered through a 0.45  $\mu m$  filter. Labeled IAV was frozen and stored at -80 °C.

To assess the effect of IAV labeling on virus titer, 10<sup>5</sup> A549 cells were seeded in each well of 96-well plate and cultured overnight. Next day, unlabeled IAV and IAV-AF568 stocks were serially diluted with DMEM supplemented with 2% FBS (DMEM/2% FBS) and spinoculated onto A549 cells at 4°C, 1500xg for 30 minutes. Cells were washed with fresh medium to remove unbound viruses and cultured in DMEM/2%FBS at 37°C for ~20 hours. Cells were then fixed with 4% PFA (ThermoFisher) for 15 min at room temperature, permeabilized with 0.3% Triton X-100 for 15 min, blocked with 10% FBS for 1 hour, and incubated with 10 µg/mL of Influenza A NP antibody at room temperature for 2 hours, followed by labeling with 2 µg/mL of Goat anti-Rabbit IgG-FITC antibody at room temperature for 45 min. Cell nuclei were labeled with 10 µM of Hoechst 33342 at room temperature for 10 min. Immunostained cells were imaged with BioTek Cytation 5 Cell Imaging Multimode Reader (BioTek Instruments, Agilent Technologies, USA). The infected cells were counted to determine the viral titer.

#### 2.4 Western blotting

Cells and viruses were harvested and processed, as described elsewhere (37). Samples containing equal amounts of p24 were used for Western blotting. Proteins were detected with rabbit anti-IFITM3, rabbit anti-IFITM1, mouse anti-FLAG, mouse anti-Ubiquitin (P4D1, Santa Cruz), anti-p24 capture antibody 183-H12-5C (CA183) was obtained from the NIH HIV Reagent Program, rabbit anti-IAV WSN HA R2376 polyclonal antibody (a gift of Dr. David Steinhauer, Emory University), or mouse anti-GAPDH (Proteintech) antibodies goat anti-human IgG HRP (ThermoFisher Scientific), mouse anti-rabbit IgG HRP (Millipore, USA), using a chemiluminescence reagent from Cytiva (Marlborough, MA, USA). The chemiluminescence signal was detected using an XR+ gel doc (Bio-Rad, Hercules, CA, USA). Densitometry was performed using Image lab (version 3.0, Bio-Rad).

#### 2.5 BlaM virus-cell fusion assay

The  $\beta$ -lactamase (BlaM) assay for virus–cell fusion was carried out in a modified version of a previously described method (37). Briefly, cells were pretreated with the respective drug at given concentration for 90 minutes, after which the pseudovirus bearing respective envelope glycoprotein and  $\beta$ -lactamase fused to Vpr (BlaM-Vpr) was bound to the target cells plated in black clear-bottom 96-well plates by centrifugation at 4°C for 30 min at 1550× g. Unbound viruses were removed by washing, and fusion was initiated by shifting cells to 37°C, 5% CO<sub>2</sub> for 120 min, after which time cells were loaded with the CCF4-AM BlaM substrate (Life Technologies). The cytoplasmic BlaM activity (ratio of blue to green fluorescence) was measured after overnight incubation at 12°C,

using a Synergy HT fluorescence microplate reader (Agilent Bio-Tek, Santa Clara, CA, USA). Cell viability was determined using the Cell Titer-Blue Reagent (Promega); after adding this reagent to cells, the samples were incubated for 30 to 60 min at 37°C, 5%  $\rm CO_2$ , and cell viability was measured on a Synergy HT plate reader ( $\rm 579_{Ex}/584_{Em}$ ).

#### 2.6 Infectivity assay

TZM-bl cells were seeded in black, clear-bottom 96-well plates and infected with serially diluted pseudoviruses in the presence or absence of CsA (20  $\mu$ M) at 37 °C for 1.5 hours, after which time, CsA was removed and replaced with fresh growth medium. Infectivity was assessed 48 h post-infection by lysing the cells with Bright-Glo luciferase substrate (Promega, WI, USA), followed by immediate measurement of luminescence using a TopCount NXT reader (PerkinElmer, CT, USA). Luminescence values were normalized to p24 content. Statistical analysis was performed using unpaired Student's t-test in GraphPad Prism v9.3.1 (GraphPad Software, CA, USA).

## 2.7 Endocytosis inhibition by pharmacological drugs

For dextran uptake assay, A549.IFITM1-C-FLAG cells were preincubated with DMSO, EIPA (50  $\mu\text{M})$  or Dynasore (120  $\mu\text{M})$  for 30 min. We added 150  $\mu\text{g/mL}$  tetramethylrhodamine dextran (TMR-dextran, ThermoFisher Scientific, D1818, 70,000 MW) to cells and incubated at 37°C for 30 min. Dynasore treated cells were kept in serum-less medium.

For transferrin uptake measurements, A549.IFITM1-C-FLAG cells were pretreated with DMSO, EIPA or Dynasore. Dynasore treated cells were kept in serum-free medium. Cells were kept on ice for 5 min, and Transferrin-fluorescein (Transferrin from Human Serum, Fluorescein Conjugate, ThermoFisher Scientific, T35352, 50 µg/mL) was added and incubated on ice for 15 min. Unbound transferrin was removed by two PBS washes, and the cells were placed at 37°C for 10 min. EIPA or Dynasore were maintained in medium throughout the experiment (during preincubation, washing, and post-incubation). Cells were transferred to ice, chilled for 5 minutes, washed with PBS and fixed with 4% paraformaldehyde. Samples were blocked using 10% FBS for 30 minutes and stained with anti-Flag antibody conjugated with AF-647.

For CsA co-treatment, cells were preincubated in fresh medium for 45 minutes. After that, cells were transferred on ice and allowed to cool down for 5 minutes prior the 30 minutes pharmacological drug and EGF treatment and anti-Flag antibody conjugated with AF-647, after which the medium was changed for DMSO- or CsA-containing medium and cells were shifted to 37C for 30 minutes. After this, cells were washed with PBS (containing respective drug) and fixed with 4% paraformaldehyde. Samples were blocked using

10% FBS for 30 minutes and stained with Wheat Germ Agglutinin (WGA) AF568 Conjugate (Fremont, CA, 29077-1) to label the cell membrane. Fluorescence intensity was measured using a 561 nm laser line for Dextran-TMR or transferrin-fluorescein AF-555, and a 633 nm laser line for WGA imaging.

### 2.8 Immunostaining, microscopy, live cell imaging, and image analyses

One day before imaging, cells were plated in 8-well chamber coverslips (Nunc, Rochester, NY, USA) coated with 0.2 mg/mL collagen (Cat. C9791, Sigma). Cells were treated with indicated compounds/inhibitors or left untreated, fixed with 4% PFA (ThermoFisher Scientific) for 20 min at room temperature, permeabilized with 150 µg/mL digitonin or 0.1% Triton X-100 for 20 min, and blocked with 10% FBS for 30 min. Cells were next incubated with respective primary antibodies diluted in 10% FBS for 1.5 h, washed, and incubated with secondary antibodies in 10% FBS for 45 min. Samples were stained with Hoechst 33342 (4 µM, Invitrogen) in PBS for 5–10 min before imaging.

Cells used for consecutive permeabilization by digitonin and Triton X-100 were treated with DMSO or CsA (20  $\mu$ M) for 90 minutes, fixed with 4% PFA for 20 min at room temperature, permeabilized with 150  $\mu$ g/mL digitonin, and blocked with 10% FBS for 30 min. Cells were next incubated with anti-IFITM3 antibodies diluted in 10% FBS for 1.5 h, washed, and incubated with anti-rabbit secondary antibodies conjugated with AF647 in 10% FBS for 45 min. Next, cells were permeabilized with 0.1% TX-100 for 20 min and blocked with 10% FBS for 30 min. Cells were next incubated with anti-IFITM3 antibodies diluted in 10% FBS for 1.5 h, washed, and incubated with anti-rabbit secondary antibodies conjugated with AF568 in 10% FBS for 45 min. Cell nuclei were stained with Hoechst 33342 (4  $\mu$ M, Invitrogen) in PBS for 5–10 min before imaging.

For live cell imaging, cells were seeded on collagen-coated glass-bottom dishes (MatTek, Ashland, MA) day before the experiment in phenol red-less medium. The next day, cells were chilled on ice and incubated with anti-Flag antibody conjugated with AF-647 for 30 minutes. After that, cells were incubated in the presence of Hoechst 33342 (4  $\mu M$ , Invitrogen) for 10 min before imaging at room temperature, washed with pre-warmed Live Cell Imaging Solution (LCIS, Invitrogen) twice. Cells in 1 ml of LCIS were moved to a prewarmed microscope chamber and allowed to equilibrate at 37°C before 1 ml of LCIS containing either DMSO or 50  $\mu M$  of CsA was added. The acquired time-lapse (acquisition every 10 second) Z-stack (10) images were converted to maximum intensity projections.

Images were acquired on a Zeiss LSM 880 confocal microscope using a plan-apochromat 63×/1.4NA oil objective. The entire cell volume was imaged by collecting multiple Z-stacks. Images were analyzed using FIJI (38). Protein signal colocalization (using both Pearson's and Mander's coefficients) was computed by the JaCoP FIJI plugin (39) on maximum-intensity projection images. For 3D analysis, individual Z-stacks capturing the bottom half of the cells were analyzed using the JaCop FIJI plugin.

#### 2.9 CsA/EGF CHX chase protocol

Cells were incubated in the presence or absence of 10  $\mu$ g/mL CHX for 1 hour at 37°C, placed on ice, and treated with combinations of CHX with CsA (20  $\mu$ M) or EGF (50 ng/mL) in HEPES-buffered medium for 30 minutes on ice. Cells were shifted to 37°C for various times before fixation with 4% PFA, permeabilization with digitonin, and immunostaining.

#### 2.10 STED imaging and analysis

Cells were incubated in the presence of 10  $\mu$ g/mL CHX for 1 hour at 37°C, placed on ice, and treated with HEPES-buffered medium containing combinations of CHX and CsA (20  $\mu$ M) or CHX and EGF (50 ng/mL) for 30 minutes. Cells were shifted to 37°C for 1 hour before fixation with PFA, permeabilization with 0.1% TX-100, and subsequent staining using respective primary followed by secondary antibodies conjugated to STED-compatible fluorophores.

In IFITM3-iSNAP and IAV imaging experiments, A549.IFITM3-iSNAP cells were pre-incubated with DMSO or 20  $\mu M$  of CsA for 1.5 hours and spinoculated with AF-568 labeled IAV at MOI of 2 at 4°C, 1500x g for 30 minutes. Infection was allowed to proceed for 1 hour in the presence of DMSO or CsA, at which time, cells were stained with SNAP-Cell 647-SiR for 30 min, washed and incubated with fresh medium for additional 30 min to remove unbound dye. Cells were fixed with 4% PFA for STED superresolution microscopy.

STED Facility Line super-resolution microscope (Abberior) on an inverted Olympus IX83 body using 60×/1.42NA oil objective, two excitation laser lines (561 nm and 640 nm), and two pulsed STED lasers (595 nm and 775 nm, respectively) were used for imaging. The entire volume of selected endosomes was imaged by collecting multiple Z-stacks at 50 nm intervals, with a pixel size of 50 nm. Line histograms across endosomes were drawn, and histograms of normalized intensity were used to assess IFITM3 or IFITM1 and EGFR distribution within endosomes. Endosomal IFITM3-iSNAP and IAV particles were segmented in 3D by MorphoLibJ Fiji plugin, and the distance between individual IAV and the center of the endosome was measured by 3D manager Fiji plugin and normalized to the endosome's radius.

#### 2.11 Site-directed mutagenesis

For site-directed mutagenesis of H27 residue, the following primers were used: H27Q-forward (5'-CAA GGA GGA GCA GGA GGT GGC), H27Q-reverse (5'-GCC ACC TCC TGC TCC TCC TTG), pQXCIP-Age-forward (5'-GCG GCC GCA CCG GT), and pQXCIP-BamHI-EcoRI-reverse (5'-GGG GCG GAA TTC CCG GAT CC). The pQXCIP-IFITM3 plasmid encoding human IFITM3 was used as a template.

#### 2.12 Pull-down experiment

The pull-down protocol has been described elsewhere (35). Briefly, cells were treated with DMSO or CsA (20  $\mu$ M) for 90 minutes, washed with PBS, and harvested/lysed using RIPA buffer without SDS. The samples were precleared with Protein G/Protein A beads (IP05-1.5ML, Millipore Sigma), incubated with the anti-IFITM3 antibody (EPR5242) overnight at 4°C. The next day, Protein G/Protein A beads were added to samples and incubated for 1 hour. Beads were washed three times with RIPA buffer, and samples were subjected to SDS-PAGE analysis and blotted using the anti-IFITM3 antibody (EPR5242), anti-Ubiquitin antibody (P4D1, sc-8017, Santa Cruz Biotechnology), or the SUMO1 monoclonal antibody (21C7, 33-2400, ThermoFisher Scientific  $^{TM}$ ).

#### 2.13 Statistical Analysis

Unpaired Student's t-test or Mann-Whitney test using GraphPad Prism version 9.3.1 for Windows (GraphPad Software, La Jolla, CA, USA), as indicated.

#### 3 Results

# 3.1 CsA treatment renders a large pool of IFITMs inaccessible to antibodies in mildly permeabilized cells

We have previously shown that pretreatment of A549 cells ectopically expressing IFITM3 with a combination of cycloheximide (CHX) and CsA rescues IAV fusion with these cells without significantly reducing the level of IFITM3 assessed by Western blotting (32). Inhibition of IFITM3 synthesis with CHX alone cleared the Golgi from the newly synthesized protein but did not alter the peripheral IFITM3 signal associated with the intracellular vesicles and the plasma membrane. Surprisingly, a combination of CsA and CHX caused a marked loss of IFITM3 signal in immunofluorescence experiments, using the monoclonal antibody EPR5242 that recognizes the N-terminal segment of IFITM3 (Figures 1A, B, Supplementary Figure S1). This is in stark contrast with the Western blotting results, showing no effect of pretreatment with CsA, CHX or their combination on IFITM3 levels [Figure 1C, (32)]. Note that treatment with CsA alone resulted in a significant loss of IFITM3 signal in immunostained samples.

The marked discrepancy between the level of IFITM3 upon combined CsA and CHX assessed by Western blotting (Figure 1C) and by an indirect immunofluorescence assay (Figures 1A, B) in digitonin-permeabilized cells implies that antibodies against the N-terminal segment of IFITM3 fail to detect the vast majority of IFITM3 molecules. Digitonin forms cholesterol-dependent pores in membranes and, thus, less efficiently permeabilizes cholesterol-poor

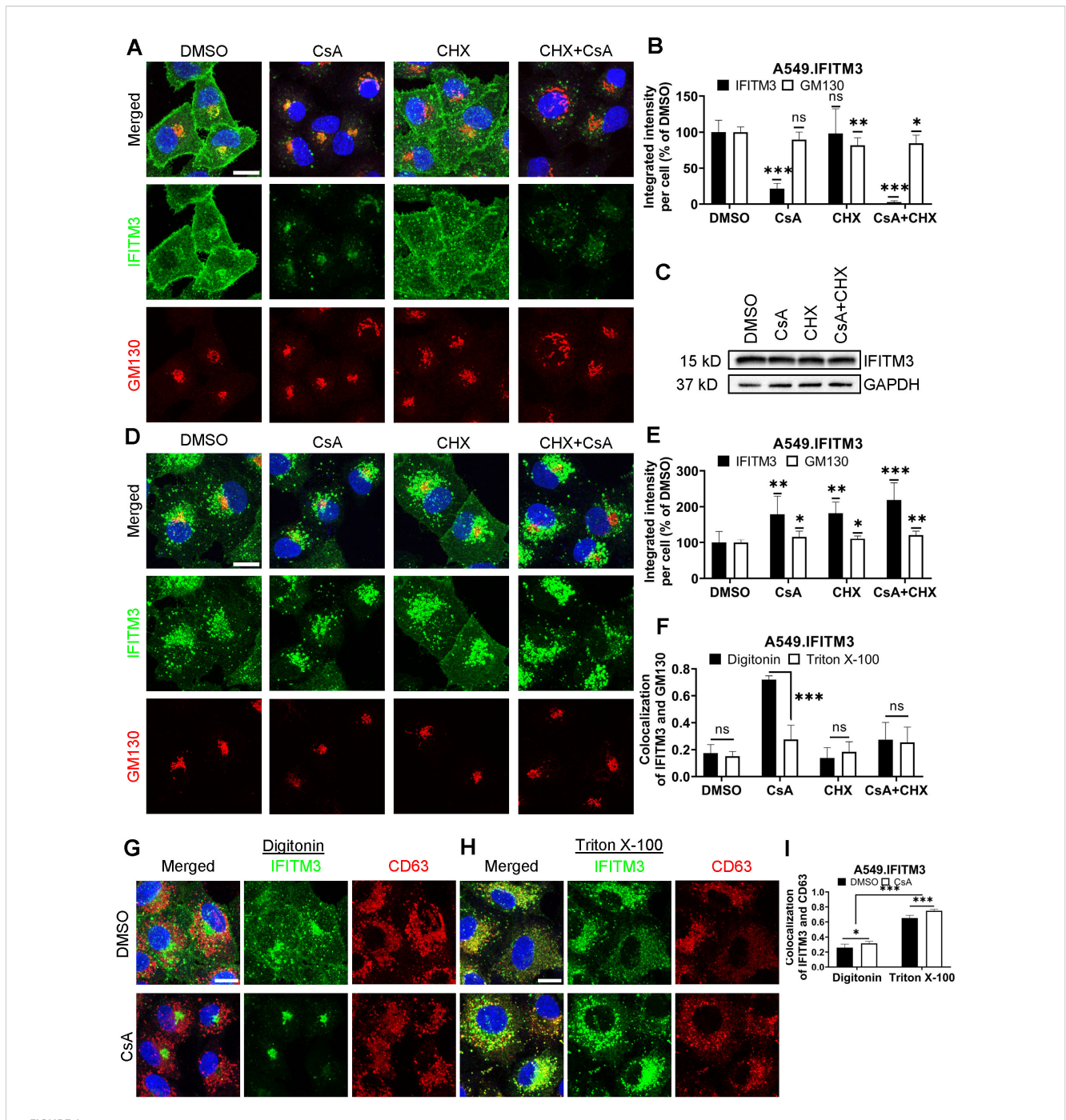


FIGURE 1
CsA treatment limits antibody access to IFITMs in digitonin-permeabilized cells. (A) A549.IFITM3 cells were treated with DMSO, CsA (20  $\mu$ M), CHX (10  $\mu$ g/mL), or a combination of CsA and CHX for 90 minutes, fixed, permeabilized with digitonin, and stained with anti-N-terminus of IFITM3 and anti-GM130 antibodies. (B) The integrated intensity of both signals per cell was measured and normalized to DMSO control. (C) Cells were treated as in (A), harvested, and cell lysates were analyzed by Western blotting. (D) A549.IFITM3 cells were treated as in (A), fixed, permeabilized with TX-100, and stained for IFITM3 and GM130. (E) Integrated intensities of IFITM3 and GM130 per cell normalized to DMSO control were calculated. (F) Colocalization of IFITM3 and GM130 signals was measured by calculating the Pearson's coefficient. (G, H) A549.IFITM3 cells were treated either with DMSO or CsA (20  $\mu$ M) for 90 minutes, fixed, permeabilized with either digitonin (G) or TX-100 (H), and immunostained for IFITM3 and CD63. Scale bars in A, D and G are 10  $\mu$ m. (I) Colocalization of IFITM3 and CD63 signals was calculated as in (F). Data are means and S.D. of two independent experiments, each acquiring three fields of view. \*p < 0.05; \*\*p < 0.01; \*\*\*p < 0.001; ns, not significant.

membranes (40). Cell permeabilization using a harsher permeabilizing agent, Triton X-100 (TX-100), which is largely independent of the lipid composition [reviewed in (40, 41)], revealed a robust IFITM3 signal are apparently associated with

endosomes (Figures 1D, E and see below). This signal is not considerably affected by CsA or CsA/CHX treatment. Such a change in subcellular distribution is specific to IFITMs, since CsA/CHX treatment does not cause notable changes in the

distribution or abundance of the Golgi markers, GM130 (Figures 1A, B, D, E), Rab6, or TGN46 (Supplementary Figure S2).

The observed discrepancy in IFITM localization and abundance under different permeabilization conditions is not caused by IFITM3 overexpression in A549 cells. Similar effects of CsA treatment on the subcellular distributions of IFITM3 were observed in digitonin and TX-100-permeabilized HeLa cells endogenously expressing IFITM3 (Supplementary Figure S3).

To delineate the impact of membrane-permeabilization protocols on the apparent subcellular distribution of IFITM3 in CsA-treated cells, we used different permeabilizing agents (Supplementary Figures S4, S5). Streptolysin O, melittin, Tween20, and organic solvents (acetone and methanol) revealed various degrees of Golgi-associated IFITM3 signal in the presence of CsA (Supplementary Figures S4-S6). On the other hand, NP-40 permeabilization resulted in IFITM3 distribution that resembled that of TX-100. Thus, the apparent subcellular distribution of IFITM3 in CsA-treated cells is dependent on the harshness of membrane permeabilization.

We next assessed the impact of CsA treatment on the colocalization of IFITM3 with the late endosomes, where this protein normally accumulates (1, 42, 43). A549.IFITM3 cells were permeabilized with digitonin or TX-100 and immunostained for IFITM3 and the marker for late endosomes, CD63 (44–46). Whereas IFITM3 and CD63 poorly colocalized in digitonin-permeabilized cells treated with DMSO or CsA (Figures 1G, I), these proteins colocalized well in TX-100 permeabilized cells exhibiting IFITM3 puncta distributed throughout the cells (Figures 1H, I). We have observed a modest but significant increase in colocalization of these proteins in CsA-treated samples, regardless of the permeabilization protocol. We also analyzed individual Z-stacks to minimize fortuitous colocalization due to signal overcrowding in maximum intensity projections (Supplementary Figures S7A-C).

To further verify that antibody access to the N-terminus of IFITM3 after CsA treatment is achieved through TX-100 treatment, but not digitonin permeabilization, we employed a two-step permeabilization and immunostaining protocol illustrated in Supplementary Figure S8A. First, A549.IFITM3 cells were permeabilized with digitonin, and accessible IFITM3 epitopes were saturated with rabbit anti-IFITM3 antibody, followed by staining with secondary goat anti-rabbit antibodies. Next, cells were treated with TX-100 and incubated with an excess of the same primary anti-IFITM3 antibody, followed by incubation with a differently labeled secondary goat anti-rabbit antibody. This protocol revealed two largely overlapping IFITM3 pools in DMSO-treated cells (Supplementary Figure S8B). However, cells pretreated with CsA contained two distinct IFITM3 pools accessible to antibodies through digitonin and TX-100 permeabilization. Whereas the IFITM3 signal after digitonin permeabilization was mainly concentrated in the perinuclear area, the additional IFITM3 signal appearing after TX-100 treatment was more peripherally distributed (Supplementary Figure S8B). After analysis of selected individual Z-stack images, we observed a change in colocalization of IFITM3 pools accessible by the respective permeabilization step.

The colocalization was higher in CsA-treated samples (Supplementary Figure S8C). In stark contrast, this 2-step immunofluorescence staining protocol did not reveal separate pools of CD63 (Supplementary Figures S8D, E). Parallel experiments using anti-IFITM3 antibodies confirmed the existence of two IFITM3 pools with different antibody accessibility in CsA-treated cells (Supplementary Figures S8F, G). Collectively, our data supports the existence of distinct pools of IFITM3 protein in CsA-treated cells, differing in their accessibility to antibodies targeting the N-terminus; however, these pools provide no insight into the functional significance or underlying cause of this variation.

## 3.2 CsA treatment occludes the IFITM's N-terminal region

The masking of the N-terminus of IFITM3 in mildly permeabilized cells co-treated with CsA/CHX (Figure 1) prompted us to test the accessibility of the C-terminus under these conditions. The absence of antibodies to a short C-terminal extracellular segment of IFITMs necessitates tagging of this protein. Since the C-terminus of IFITM3 is exposed to a degradative environment of late endosomes and lysosomes, C-terminally appended tags tend to be digested by proteases (4, 5, 26, 42, 47). We, therefore, tagged the C-terminus of the plasma membranelocalized IFITM1 that faces the extracellular milieu (48-50). A549 cells ectopically expressing IFITM1 fused with a FLAG-tag at its Cterminus (A549.IFITM1-FLAG) were treated with CsA and permeabilized with digitonin or TX-100. Samples were coimmunostained using anti-IFITM1 (N-terminus) and anti-FLAG (C-terminus) antibodies, as illustrated in Figure 2A. In control (DMSO-treated) cells permeabilized with digitonin or TX-100, the IFITM1's N- and C-terminal signals largely colocalized at the plasma membrane, as expected (Figures 2B, C). Strikingly, colocalization of the N- and C-terminal IFITM1 signals was significantly reduced in CsA-treated cells permeabilized with digitonin (Figure 2B). The N-terminal signal concentrated in the perinuclear/Golgi area (as previously observed (32)), while the Cterminal signal appeared punctate, consistent with endosomal localization (Figure 2B). By contrast, CsA-treated cells permeabilized with TX-100 exhibited good colocalization of Nand C-terminal signals that presumably localized to endosomes (Figures 2C, D). We also analyzed individual Z-stacks to minimize fortuitous colocalization of abundant IFITM and CD3 signals in maximum intensity projection images (Supplementary Figure S7D). This analysis confirmed our initial observation of lower colocalization of N- and C-termini in digitonin-permeabilized cells after treatment with CsA compared to DMSO-treated cells; a higher colocalization was observed in TX-100-permeabilized cells.

To test if IFITM1 relocalizes to late endosomes in the presence of CsA, A549.IFITM1-FLAG cells were pretreated with DMSO or CsA, permeabilized with digitonin or TX-100, and co-stained for CD63 and either IFITM1 N-terminus (using anti-IFITM1 antibody, Supplementary Figures S9A-C) or C-terminus (using anti-FLAG

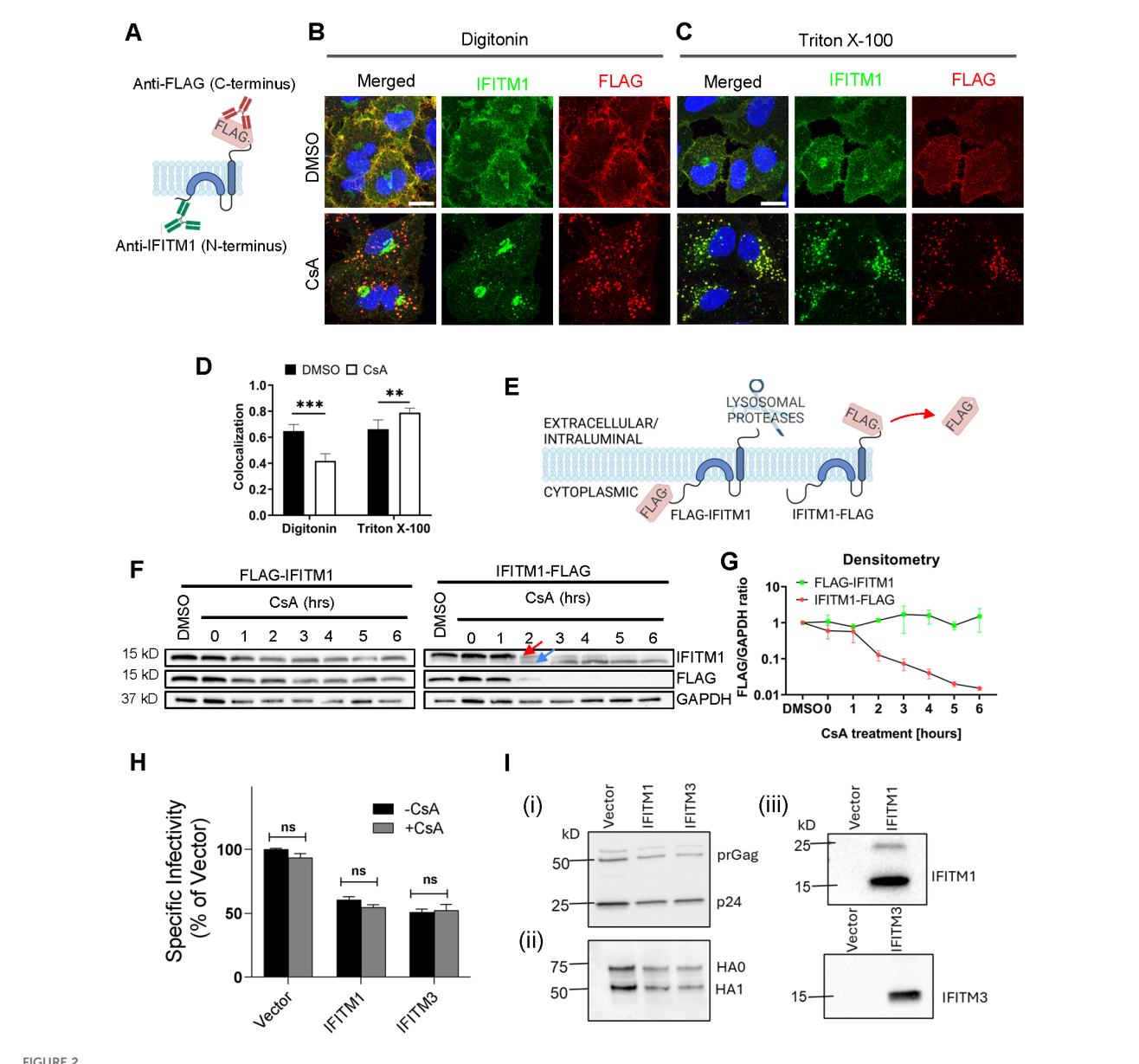


FIGURE 2
Disparate immunostaining patterns of the IFITM1's N- and C-termini following CsA-treatment. (A) Illustration of a dual immunostaining strategy of IFITM1 fused to FLAG-tag at its C-terminus (IFITM1-FLAG). Not drawn to scale. (B, C) A549.IFITM1-FLAG cells were treated with DMSO or CsA (20 μM) for 90 minutes, fixed, permeabilized with either digitonin (B) or TX-100 (C), and stained using anti-IFITM1 (N-terminus, intracellular) or anti-FLAG (C-terminus, extracellular) antibodies. Scale bar 10 μm. (D) Colocalization of the IFITM1 N-terminus and C-terminal FLAG signals calculated using Mander's overlap coefficient (MOC). Data are from two independent experiments. \*\*p < 0.01; \*\*\*p < 0.001. (E) Illustration of IFITM1 protein with the FLAG-tag appended to the N-terminus (FLAG-IFITM1) or to the C-terminus (IFITM1-FLAG) and anticipated FLAG tag proteolysis in endolysosomes. (F) A549 cells ectopically expressing FLAG-IFITM1 or IFITM1-FLAG proteins were treated with DMSO or CsA (20 μM) for indicated times, harvested, and the cellular levels of IFITM1 and FLAG were assessed by Western blotting. (G) densitometry analysis of FLAG signal abundance (normalized to loading control, GAPDH). Red arrow points to the IFITM1-FLAG band, blue arrow points to the untagged IFITM1 band. (H) A panel of pseudoviruses (Vector, IFITM1, and IFITM3) was generated by transfecting HEK293T/17 cells. TZM-bl cells were infected with control pseudoviruses bearing Influenza A virus hemagglutnini (HA) and neuraminidase or pseudoviruse bearing either IFITM1 or IFITM3 in the presence or absence of CsA (20 μM). Luciferase activity was measured at 48 hours post-infection and normalized to the Vector control. Data represent mean ± SD from triplicate wells across two independent experiments. (I) Western blotting to verify: (i) virus production and Gag cleavage to produce p24; (ii) HA processing and incorporation into pseudoviruses; and (iii) IFITM protein incorporation into virions. See also Supplementary Figure S12.

antibody, Supplementary Figures S9D-F). In CsA-treated and digitonin-permeabilized cells, the N-terminal signal was largely concentrated in the perinuclear area, while the N- and C-terminal IFITM1 signals colocalized well with CD63 in TX-100 permeabilized CsA-treated cells (Supplementary Figures S9B, E).

The IFITM1 C-terminus remains accessible to antibodies in digitonin-permeabilized cells. These observations led us to conclude that IFITM proteins are transported to late endosomes, where the N-terminus becomes poorly accessible to antibodies in mildly permeabilized cells through a yet unknown mechanism. Of

note, CsA-induced IFITM relocalization to late endosomes was not associated with an altered ubiquitination or SUMOylation (Supplementary Figure S10).

## 3.3 CsA treatment does not change the IFITM's membrane topology

Poor accessibility of the IFITMs' N-terminal segment in CsA-treated cells might be caused by changes in the protein's structure and/or topology. It is generally accepted that IFITMs are single-span type II transmembrane proteins, with the N-terminus facing the cytosol and the C-terminus exposed to the extracellular milieu (IFITM1) or the lumen of endosomes (IFITM-2 and -3) (48, 51). Although this model is generally accepted, some studies suggested alternative topologies, including the inverted topology, with the N-terminus of IFITM proteins facing the extracellular space or lumen of endosomes (52, 53).

To test possible CsA effects on IFITM1's topology, we examined proteolysis of the N- and C-terminal FLAG tags by Western blotting. This approach takes advantage of the IFITM1's Cterminal tag cleavage by endosomal proteases after CsA-induced redistribution from the plasma membrane to late endosomes (Figure 2E). We reasoned that a flipped topology would lead to clipping of the N-terminal FLAG tag by endosomal proteases. Cell lysates were analyzed by SDS-PAGE and blotted using anti-IFITM1 and anti-FLAG antibodies to distinguish protein degradation from selective FLAG cleavage. In both cell lines expressing N- and Cterminal FLAG-tagged IFITM1, a modest degradation of the IFITM1 protein was detected after a prolonged CsA treatment (Figure 2F). However, only IFITM1-FLAG exhibited loss of FLAG signal in CsA-treated cells after 1 hour of treatment, with complete loss of FLAG signal after 3 hours. Loss of the FLAG tag was manifested by a concomitant increase in the IFITM1 band's mobility (Figure 2F, arrows), as expected. Importantly, we did not detect loss of the N-terminal FLAG tag at any point after CsA treatment (Figure 2G).

To further probe possible changes in IFITM's topology, we incubated A549.IFITM1-FLAG cells with CsA overnight and chased in a CsA-free growth medium which lacked or contained CHX to block protein synthesis, as shown in Supplementary Figure S11A. After incubation for up to 6 hours, samples were harvested and examined by Western blotting. We observed a slow recovery of the FLAG signal with a concurrent shift of an untagged IFITM1 band to a FLAG-tagged IFITM1 band starting at 3 hours after CsA removal (Supplementary Figure S11B). As expected, the FLAG signal recovery was blocked in the presence of CHX. Together, these results argue against possible CsA-induced changes in IFITM's topology.

To verify that clipping of C-terminal FLAG occurs in endolysosomes, we co-treated cells with CsA and either the lysosomal pathway inhibitors, Bafilomycin A1 (BafA1) and NH<sub>4</sub>Cl, or proteasomal degradation inhibitors, MG132 and Lactacystin. Cells were also co-treated with a pan-cathepsin inhibitor, E64-d. Co-treatment with CsA/BafA1 or CsA/NH<sub>4</sub>Cl

abrogated the IFITM1's mobility shift and concomitant loss of FLAG signal (Supplementary Figure S11C). By comparison, partial inhibition was observed in cells co-treated with a non-specific proteasome inhibitor, MG132, while co-treatment with a more specific inhibitor Lactacystin did not inhibit FLAG removal from IFITM1. Inhibition of lysosomal cathepsins by E64-d showed only partial inhibition on CsA-driven loss of FLAG signal (Supplementary Figure S11C). The activity of MG132 and Lactacystin was confirmed by blotting using an anti-ubiquitin antibody. As expected, both MG132 and Lactacystin induced the accumulation of ubiquitinated proteins due to the block of the proteasomal pathway (Supplementary Figure S11C).

The above results show that the C-terminus of IFITM1 in CsA-treated cells is facing the lumen of late endosomes, implying that the topology of this protein is not altered compared to cells' basal condition.

To further test the notion that CsA rescues IAV fusion with IFITM-expressing cells by relocalizing these proteins, we asked whether CsA can directly antagonize IFITM's antiviral activity. Here, we took advantage of reduction of IAV pseudovirus infectivity by virus-incorporated IFITMs (54, 55). IFITM1 and IFITM3 incorporation into IAV pseudoviruses (verified by Western blotting, Figure 2I, Supplementary Figure S12) modestly reduced their specific infectivity compared to control viruses (Figure 2H, Supplementary Figure S12), without significantly modulating the HA glycoprotein processing or incorporation into virions (Figure 2I, Supplementary Figure S12). Importantly, and in stark contrast to the CsA effect on virus restriction in IFITMexpressing cells ((32) and Figure 3A), CsA did not alter the specific infectivity of IFITM-containing IAV pseudoviruses (Figure 2H, Supplementary Figure S12). This finding argues against the possibility of direct CsA antagonism with the antiviral activity of IFITMs.

#### 3.4 CsA rescues IAV fusion with IFITMexpressing cells through a mechanism that is distinct from those of rapamycin and MK-2206

As reported previously by us and others (29, 30, 32), rapamycin antagonizes the IFITM3's antiviral activity. Shi et al. concluded that rapamycin leads to IFITM3 degradation through inhibition of mTOR and subsequent phosphorylation of TFEB, the master regulator of lysosome function and microautophagy. However, this effect seems to require the N-terminus of IFITM3, since rapamycin fails to promote degradation of the  $\Delta 17$ -20 IFITM3 mutant, which lacks the YEML endocytic motif, localizes to the plasma membrane, and restricts a different set of viruses (30). Indeed, the IAVpp fusion block was relieved by rapamycin in A549.IFITM3 cells but only partially recovered in A549.IFITM1-FLAG cells (Figure 3A).

During our screening of inhibitors of various cellular pathways that might antagonize IFITM3, we found that the Akt inhibitor, MK-2206, rescued IAV-cell fusion in A549.IFITM3 cells (Figure 3A). Note that

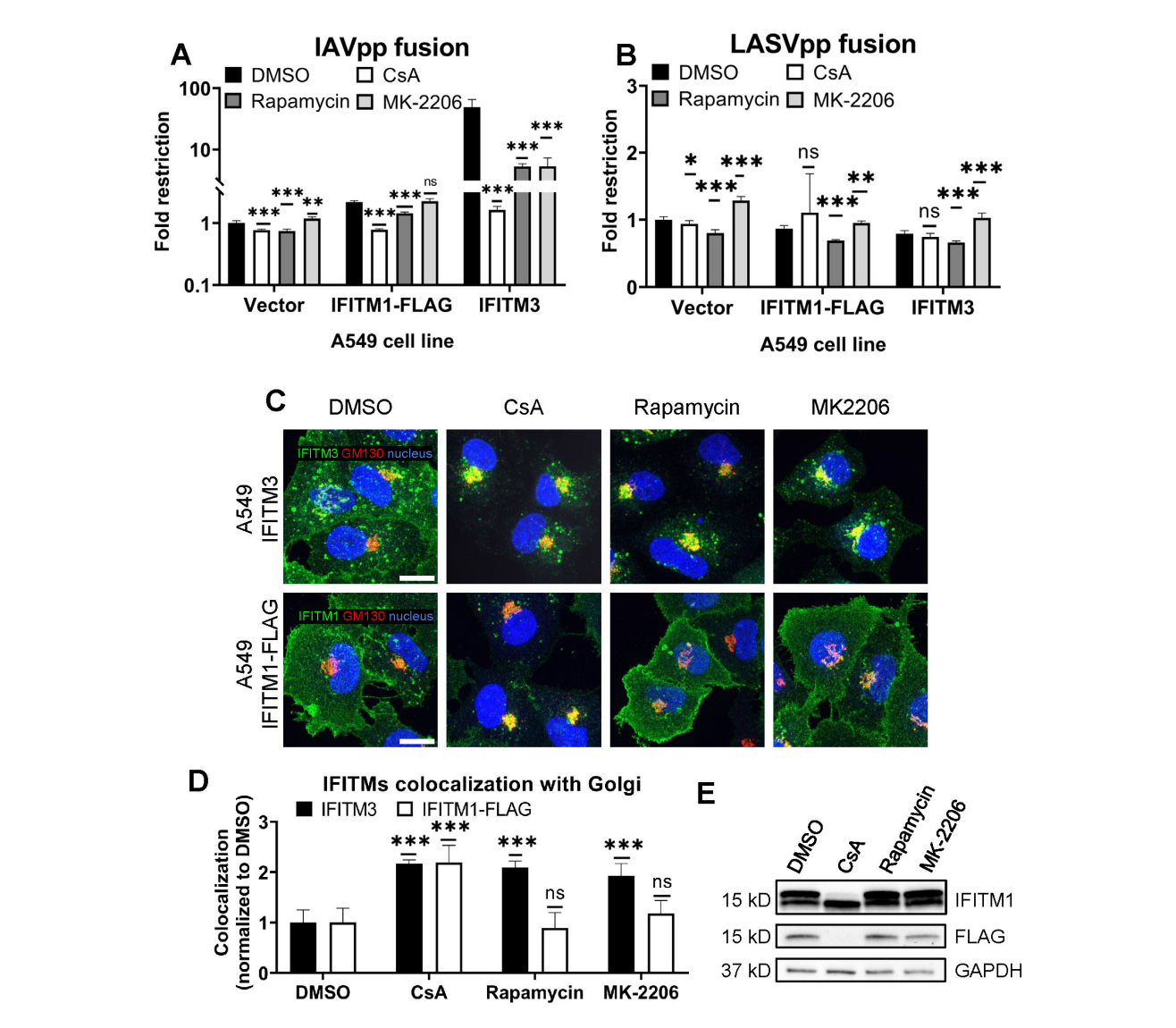


FIGURE 3
CsA-induced rescue of IAV fusion with IFITM1 expressing cells occurs through a mechanism that is distinct from those of rapamycin and MK-2206. (A, B) A549.Vector, A549.IFITM3 or A549.IFITM1-FLAG cells were preincubated in the presence of DMSO, CsA (20  $\mu$ M), rapamycin (20  $\mu$ M), or MK-2206 (10  $\mu$ M) for 90 minutes and challenged with IAVpp (A) or LASVpp (B) pseudoviruses, and viral fusion was measured using a beta-lactamase assay. (C) A549.IFITM3 or A549.IFITM1-FLAG cells were treated as in (A), fixed, stained for GM130 and respective IFITM proteins, and imaged. Scale bar 10  $\mu$ m. (D) Colocalization between IFITMs and GM130 in cells shown in (C) was calculated using MOC. (E) A549.IFITM1-FLAG cells were treated as in (A), harvested, and cell lysates were analyzed by Western blotting. Data are means and S.D. of two independent experiments, each performed in triplicate. \*p < 0.05; \*\*p < 0.01; \*\*\*p < 0.001; ns, not significant.

both rapamycin and MK-2206 had non-specifically modulated fusion of LASV pseudoviruses, which are resistant to IFITM-mediated restriction (1) (Figure 3B). This effect may be due to inhibition of the PI3K/AKT/mTOR pathway. We also observed a modest, yet statistically significant, drop in viability in cells treated with the above compounds (Supplementary Figure S13). Interestingly, unlike CsA, neither rapamycin nor MK-2206 induced relocalization of IFITM1-FLAG protein from the plasma membrane, while both successfully altered the subcellular distribution of IFITM3 (Figures 3C, D). Finally, only CsA treatment of A549.IFITM1-FLAG cells caused loss of FLAG and concomitant shift in IFITM1 band mobility on immunoblots (Figure 3E).

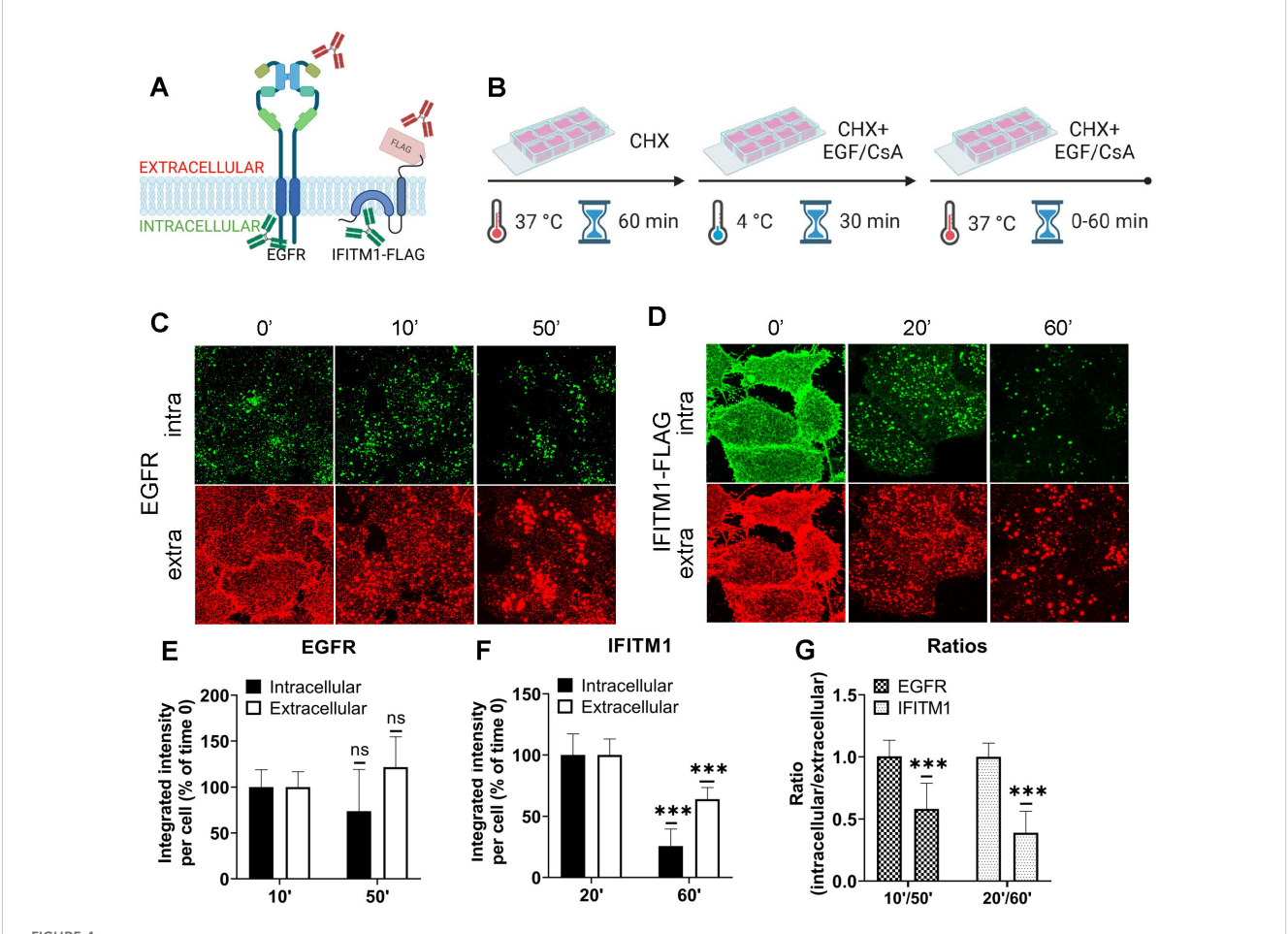
Taken together, our data suggests a fundamentally different mechanism of CsA action on IFITMs that, in contrast to rapamycin and MK-2206, modulates the subcellular distribution of both IFITM3 and IFITM1 and potently enhances virus-cell fusion.

## 3.5 CsA treatment sequesters IFITMs inside late endosomes, likely within intraluminal vesicles

Our results (Figures 1, 2) reveal that CsA treatment relocalizes IFITM1 to late endosomes, while, except for the newly synthesized

pool of IFITM3, this protein remains largely endosome associated. In both cases, CsA treatment leads to selective masking of the protein's N-terminus in cells permeabilized with digitonin, without a change in IFITM's membrane topology. This surprising observation can be explained by IFITM1 and IFITM3 redistribution from the PM and the limiting membrane (LM) of late endosomes, respectively, to intraluminal vesicles (ILVs) of multivesicular bodies (MVBs), which are complex and dynamic structures [reviewed in (56, 57)]. To test the notion that the inaccessibility of ILVs to digitonin is the reason for poor immunostaining of IFITMs in CsA-treated cells, we employed the epidermal growth factor receptor (EGFR) as a reference marker. EGFR is a type I transmembrane protein that is redirected from the plasma membrane to ILVs upon activation by the EGF ligand (58, 59). We took advantage of the ability to immunolabel the extracellular and intracellular domains of EGFR and IFITM1-FLAG independently to examine the accessibility of respective epitopes in digitonin-permeabilized cells (Figure 4A).

A549.IFITM1-FLAG cells were treated, as shown in Figure 4B. Briefly, cells were pretreated with CHX for 1 hour to block protein synthesis, exposed to either EGF or CsA on ice for 30 min, and shifted to 37°C. Samples were fixed at indicated times, permeabilized with digitonin, and stained for extracellular domains (N-terminus of EGFR and C-terminus of IFITM1-FLAG) and intracellular domains (C-terminus of EGFR and Nterminus of IFITM1-FLAG). The weak and dispersed signal of EGFR is likely due to the inhibition of the requisite EGFR dimerization in the cold (60, 61). The EGFR aggregation and internalization from the plasma membrane occurred within 10 minutes, while IFITM1 internalization was detectable at ~20 minutes after shifting to 37°C (Figures 4C, D). Both proteins showed a marked shift from the plasma membrane to endosomal compartments, along with strongly diminished signals of their respective intracellular domains after 60 minutes of treatment with EGF or CsA (Figures 4E-G). These data suggest that both proteins are redistributed to the ILVs upon CsA treatment, as the



The IFITMs' N-terminal region is selectively sequestered in late endosomes of CsA-treated cells. (A) Antibodies recognizing extracellular or intracellular domains of EGFR or IFITM1-FLAG proteins were used to probe the accessibility of these domains in cells treated with the EGFR ligand or CsA. Not drawn to scale. (B) A549 cells were incubated in the presence of CHX for one hour, placed on ice, treated with EGF (EGFR samples) or CsA (IFITM1 samples) for 30 minutes, and returned to 37 °C for indicated times. Cells were fixed, permeabilized with digitonin, and stained for extracellular and intracellular domains of a respective target protein, EGFR (C) or IFITM1/FLAG (D). The integrated intensity for each respective antibody targeting domains of EGFR (E) or IFITM1 (F) was calculated and plotted as a function of time of incubation. (G) The ratios between integrated intensities of intracellular and extracellular domains of EGFR and IFITM1 at indicated times are plotted. Data are means and S.D. of two independent experiments, each acquiring three fields of view. \*\*\*p < 0.001; ns, not significant.

signal of their extracellular domains weakened over time when compared to the respective signal from intracellular domains. These results support our model that, in CsA-treated cells, the extracellular domains are facing the lumen of MVBs, which is accessible to antibodies in digitonin-permeabilized cells, while the intracellular domains are hidden inside the ILVs.

We visualized the dynamics of IFITM1 internalization in the presence of CsA by directly labeling IFITM1-C-FLAG with anti-FLAG antibody conjugated to AF647 and performed live cell imaging. IFITM1 was rapidly relocalized from the plasma membrane (Movie S2), which was not observed in control experiments (Movie S1). The aggregation of IFITM1 signal in cytosolic puncta started around 10 min and culminated at 20 min.

To investigate the mechanism of CsA-induced IFITM1 internalization, inhibitors targeting macropinocytosis [EIPA (62, 63)] and dynamin-dependent endocytosis [Dynasore (64)] were employed. As expected, EIPA and Dynasore inhibited the uptake of respective cargoes - 70 kDa dextran (macropinocytosis) and transferrin (clathrin-mediated endocytosis) (Supplementary Figure S14A). Notably, Dynasore had a minimal impact on CsAinduced IFITM1 internalization, whereas EIPA significantly disrupted IFITM1 relocalization to late endosomes (Supplementary Figures S14B-D). It should be noted that EIPA did not fully block CsA-induced internalization of IFITM1, as this protein's colocalization with the plasma membrane stained with WGA was significantly reduced in EIPA/CsA samples compared to EIPA/DMSO samples (Supplementary Figure S14B). We note that co-treatment with CsA and these inhibitors—especially EIPA mildly reduced cell viability. Interestingly, our markers for macropinocytosis (Dextran) and clathrin-mediated endocytosis (EGF) showed high colocalization after 30 min of CsA treatment, suggesting that both pathways eventually converge, which is in line with published studies [reviewed in (65)].

To further test if IFITM1 is relocalized to ILVs by CsA, we employed a super-resolution stimulated emission depletion (STED) microscopy of IFITMs and EGFR, a well-established ILV marker upon ligand (EGF) binding [reviewed in (66)]. A549.IFITM1-C-FLAG cells were pretreated with CHX for 1 hour prior to incubation with a combination of CHX, EGF, and CsA (or DMSO as control) on ice for 30 minutes (similar to Figure 4B). Cells were then shifted to 37 °C for 1 hour, fixed, permeabilized with TX-100, and stained using anti-IFITM1 antibodies targeting the intracellular epitope N-terminal region of IFITM1, and anti-EGFR antibodies, targeting the extracellular epitope. While there was no colocalization between IFITM1 and EGFR signals in mock treated cells (Supplementary Figure S15A), these proteins appeared to colocalize in CsA-treated cells (Supplementary Figure S15B), suggesting a convergence of these proteins in the same pool of endosomes.

Lastly, we assessed whether CsA induces IFITM3 relocalization from the LM to ILVs using STED microscopy. A549.IFITM3 (IFITM3+) or control A549.vector (IFITM3-) cells were treated using the protocol described above for IFITM1-C-FLAG STED experiments and in Figure 4B. Cells were fixed, permeabilized with TX-100, and stained using anti-IFITM3 antibody targeting the intracellular epitope, and anti-EGFR, targeting the extracellular

epitope. In control A549.IFITM3 cells treated with DMSO, endosomes tended to have a hollow, doughnut-shaped appearance based upon the peripherally localized EGFR signal, with a diameter of  $1.2\pm0.2~\mu m$ ; IFITM3 and EGFR partially colocalized at the periphery of these endosomes (Figures 5A, E). Notably, most of the EGFR signal was punctate. In contrast, CsA treatment reduced the diameter of endosomes to  $0.68\pm0.17~\mu m$ , and these endosomes were "filled" with the IFITM3 that was no longer localized to the LM (Figures 5B, E). We did not observe enlarged endosomes or the effect of CsA on their size in IFITM3-negative control cells (Figures 5C, D, F) regardless of the treatment (0.7  $\pm$  0.2  $\mu m$  vs 0.6  $\pm$  0.2  $\mu m$  for DMSO and CsA treated cells, respectively).

Alternatively, we infected A549 cells with AF-568-labeled IAV in the presence or absence of CsA. To achieve non-invasive labeling, we used IFITM3-iSNAP in combination with SNAP-Cell 647-SiR (34). IAV was found to colocalize with the limiting membrane of late endosomes, as marked by the IFITM3-iSNAP signal (Supplementary Figure S16A). CsA-induced changes in the distribution of IFITM3-iSNAP and IAV that clearly shifted from the limiting membrane toward the center of the endosome (Supplementary Figure S16B).

#### 4 Discussion

While IFITMs play an important role in curbing viral infection, the mechanism of their antiviral activity is not fully understood. Hurdles to delineating the mechanism of IFITM action include uncertainty regarding their membrane topology and complex regulation of their subcellular localization by single residue substitutions and post-translational modifications (23–28). Pleiotropic effects of CsA on cellular processes (67–69) precluded the identification of factors/pathways regulating IFITMs' localization and antiviral activity in treated cells. The results reported in this study provide new insights into the mechanism of CsA-mediated rescue of viral fusion through regulation of IFITMs' trafficking/localization (Figure 6).

Co-treatment with CsA and CHX (to eliminate the signal from a newly synthesized IFITM pool that transits through the Golgi) revealed a large pool of both IFITM1 and IFITM3 in endosomes. Importantly, this pool is only detectable by immunofluorescence in TX-100 permeabilized cells that gain access to ILVs, whereas mild permeabilization with digitonin allows antibody access almost exclusively to the Golgi-trapped pool of IFITMs. Indeed, there is evidence that overexpressed IFITM3 accumulates in the Golgi and delays transport of other glycoproteins through this apparatus (70). The impact of CsA on IFITM1 localization is particularly striking, since unlike the endosome-localized IFITM3, IFITM1 is nearly fully relocalized to late endosomes/ILVs.

Two lines of evidence support the notion that CsA induces IFITM1 and IFITM3 redistribution from the plasma membrane and the limiting membrane of late endosomes, respectively, to ILVs. First, the N-terminus of IFITMs is selectively sequestered in intracellular compartments that are not accessible to antibodies in digitonin-permeabilized cells. This effect is similar to the

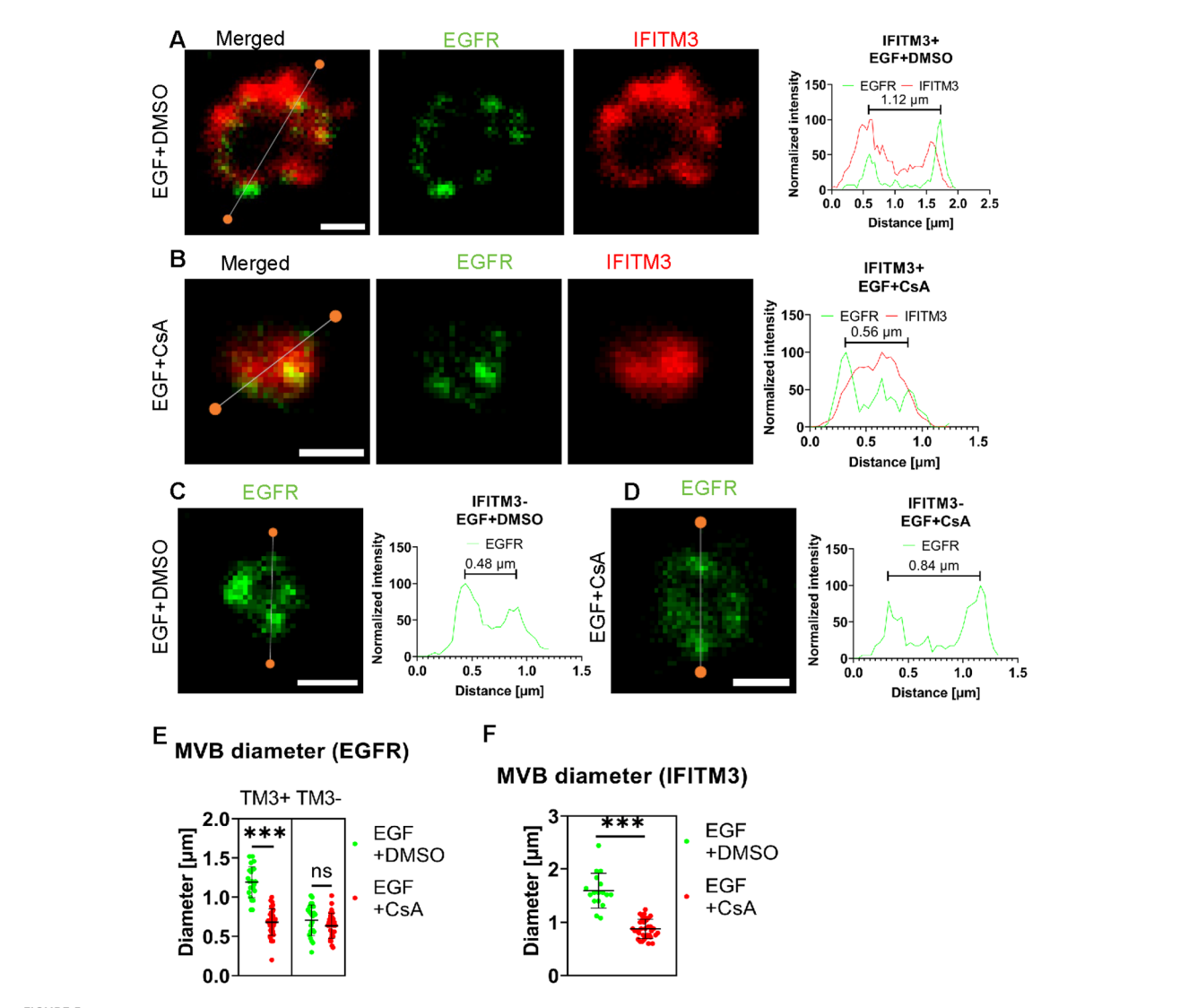
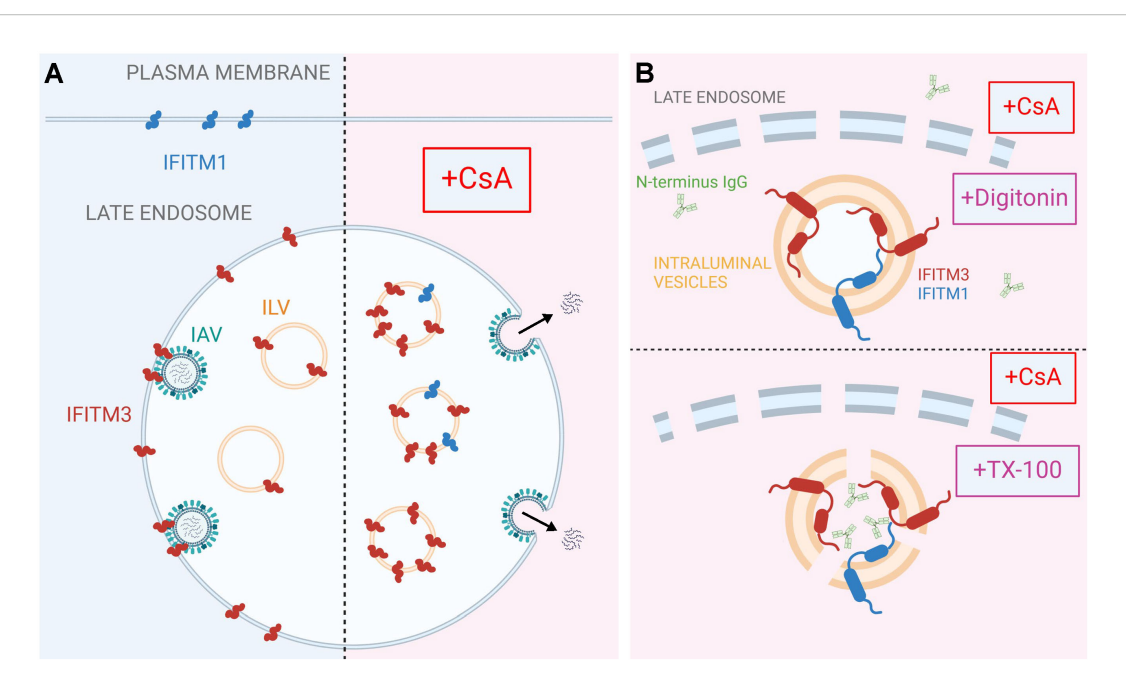


FIGURE 5

IFITM3 relocates to the interior of late endosomes upon CsA treatment. A549.IFITM3 (IFITM3+) or A549.vector (IFITM3-) cells were incubated in the presence of CHX for one hour, placed on ice, treated with EGF and either DMSO (A, C) or CsA (B, D) for 30 minutes, and returned to 37 °C for indicated times. Cells were fixed, permeabilized with TX-100, and stained using anti-EGFR (targeting N-terminus) and anti-IFITM3 primary antibodies and secondary antibodies conjugated to STED-compatible fluorophores, STAR RED and STAR 580. Normalized linear intensity profiles across endosomes are shown for each channel. To measure the endosome diameter, local maxima of EGFR signals were used. Endosomes with low EGFR signal, excessive background noise, or indistinguishable features were excluded. Representative linear histograms for IFITM3 positive or negative cells in the presence or absence of CsA are shown. (E) Endosome diameters based on EGFR signal are plotted. Endosomes from two independent experiments (n>20 endosomes, n>15 cells) were analyzed per condition and per cell line (A549.IFITM3 and A549.vector). (F) The endosome diameters based on IFITM3's signal for IFITM3+ cells were calculated based upon the distance between the normalized linear profile intensities corresponding to 25% of signal. Endosomes with a high background were omitted. Lines and bars are medians and interquartile range. Scale bar is 0.5 μm. \*\*\*p < 0.001; ns, not significant.

sequestration of the cytoplasmic tail of EGFR, a well-characterized protein targeted to ILVs upon ligand (EGF) binding (reviewed in (66)). Importantly, the lack of CsA's effect on the overall level and topology of IFITMs in A549 cells rules out partial or full cleavage of the N-terminal region recognized by the antibodies as the reason for loss of the immunofluorescence (IF) signal. Second, superresolution microscopy implies that IFITM3 is translocated from the LM of late endosomes to the lumen, and this relocalization is associated with shrinking of the endosome's diameter. This finding is also supported by our observation that the C-terminal FLAG-tag on IFITM1 is cleaved in the presence of CsA.

ILVs originate from the LM of MVBs and carry cargo destined for degradation, secretion, or temporary segregation from the cytoplasm (reviewed in (71). Importantly, IFITM1 or IFITM3 proteins trapped in ILVs after CsA treatment are not degraded for hours, as evidenced by constant levels of these proteins in cell lysates (Figure 1C). It is worth noting that endogenously expressed IFITM3 in HeLa cells treated with CsA appears to be degraded within a few hours of CsA treatment (32). The ILV formation is regulated by the ESCRT machinery, with ALIX and TSG101 playing key roles (72–74). These proteins can perform partially overlapping functions confounding the results of knockdown experiments.



A model for CsA-induced IFITM relocalization to the ILVs of late endosomes and rescue of IAV fusion. A proposed model of modulation of subcellular localization of IFITMs by CsA. (A) In the absence of CsA, IFITM1 is primarily located at the plasma membrane, while IFITM3 concentrates in the limiting membrane and intraluminal vesicles (ILVs) of the late endosome. This basal subcellular distribution of IFITM proteins inhibits the fusion of incoming viruses (e.g. IAV) with the cell membranes. CsA redirects IFITM proteins from their respective locations to the ILVs, sequestering them away from incoming viruses and allowing viral fusion to occur at the respective cellular locations. (B) Digitonin does not permeabilize ILVs, thus precluding access of antibodies to the N-terminus of IFITM proteins. In contrast, TX-100 disrupts the ILV membrane, enabling antibody binding to the N-terminus of IFITM proteins. Visual representations are not drawn to scale. Created in BioRender.com.

While the ESCRT system is central to ILV biogenesis, studies have shown ILV production in cells lacking multiple ESCRT proteins, indicating the contribution of endosomal lipids, BMP, and ceramide in ILV biogenesis (75–77). It was also reported that IFITM3 expression affects cholesterol levels and distribution, either directly (78) or through inhibition of VAMP-Associated Proteins (79).

CsA is known to partition into and alter the properties of lipid membranes, including shifting the phase transition temperature and lipid domain morphology (80-82). CsA also selectively interacts with sphingomyelin (83). Given that the antiviral activity of IFITMs is modulated by their interactions with lipids, such as cholesterol and phosphoinositides (84-87), it is conceivable that CsA can also modulate the subcellular distribution of IFITMs indirectly, through modifying the cell membranes. However, this mechanism does not fully explain how IFITM1 is transported from the plasma membrane to the LM of late endosomes and then to ILVs, suggesting the involvement of additional host cofactors. It is intriguing that rapamycin and MK-2206, both inhibitors of the PI3K/AKT/mTOR (PAM) pathway, do not impact the localization of IFITM1 or the N-terminally truncated IFITM3 lacking the endocytic signal (30). This suggests that CsA may influence multiple pathways that exert broader effects on IFITMs and cellular processes. However, the non-specific effects of PAM inhibitors, rapamycin and MK-2206, on cell viability could reduce virus-cell fusion, potentially leading to decreased fusion efficiency.

CsA-mediated redistribution of IFITMs has implications beyond viral entry and infection. IFITM proteins play a role in cancer, syncytiotrophoblast fusion, and inhibition of ILV backfusion (88–92). The rapid and non-toxic redistribution of IFITMs by CsA offers a promising means to counteract the above adverse effects of IFITMs and improve lentivirus-based gene delivery (31). Unlike Rapamycin and MK-2206, CsA successfully redistributes IFITMs, which increases its utility for modulating the adverse effects of these proteins. Future studies will be aimed at identifying the IFITM motif and cellular partners responsible for the rapid and selective translocation into ILVs. This knowledge can be utilized for a controlled sequestration of target cellular proteins into ILVs.

#### Data availability statement

The original contributions presented in the study are included in the article/Supplementary Material. Further inquiries can be directed to the corresponding author.

#### **Author contributions**

DP: Investigation, Writing – original draft, Writing – review & editing, Conceptualization, Formal analysis. YZ: Formal analysis, Writing – review & editing, Writing – original draft, Investigation.

SV: Investigation, Writing - review & editing, Formal analysis. GM: Conceptualization, Supervision, Writing – original draft, Writing – review & editing, Funding acquisition.

#### **Funding**

The author(s) declare financial support was received for the research and/or publication of this article. Research reported in this publication was supported by the NIAID R01 grant AI135806 to GM (R01 AI190198 and R37 AI150453).

#### **Acknowledgments**

The authors would like to thank the members of Melikian lab members, Mariana Marin, Gokul Raghunath, and Sergii Buth, for reading the manuscript and valuable discussions. We also wish to thank Hui Wu and Monica Macias for technical support. We are grateful to Dr. Baek Kim for access to BioTek Cytation 5.

#### Conflict of interest

The authors declare that the research was conducted in the absence of any commercial or financial relationships that could be construed as a potential conflict of interest.

#### References

- 1. Brass AL, Huang IC, Benita Y, John SP, Krishnan MN, Feeley EM, et al. The IFITM proteins mediate cellular resistance to influenza A H1N1 virus, West Nile virus, and dengue virus. *Cell.* (2009) 139:1243–54. doi: 10.1016/j.cell.2009.12.017
- 2. Diamond MS, Farzan M. The broad-spectrum antiviral functions of IFIT and IFITM proteins. *Nat Rev Immunol.* (2013) 13:46–57. doi: 10.1038/nri3344
- 3. Huang IC, Bailey CC, Weyer JL, Radoshitzky SR, Becker MM, Chiang JJ, et al. Distinct patterns of IFITM-mediated restriction of filoviruses, SARS coronavirus, and influenza A virus. *PloS Pathog.* (2011) 7:e1001258. doi: 10.1371/journal.ppat.1001258
- 4. Perreira JM, Chin CR, Feeley EM, Brass AL. IFITMs restrict the replication of multiple pathogenic viruses. *J Mol Biol.* (2013) 425:4937–55. doi: 10.1016/j.jmb.2013.09.024
- 5. Bailey CC, Zhong G, Huang IC, Farzan M. IFITM-family proteins: the cell's first line of antiviral defense. *Annu Rev Virol.* (2014) 1:261–83. doi: 10.1146/annurev-virology-031413-085537
- 6. Marziali F, Cimarelli A. Membrane interference against HIV-1 by intrinsic antiviral factors: the case of IFITMs. *Cells*. (2021) 10:1171. doi: 10.3390/cells10051171
- 7. Yánez DC, Ross S, Crompton T. The IFITM protein family in adaptive immunity. Immunology. (2020) 159:365–72. doi: 10.1111/imm.13163
- 8. Bailey CC, Huang IC, Kam C, Farzan M. Ifitm3 limits the severity of acute influenza in mice. *PloS Pathog.* (2012) 8:e1002909. doi: 10.1371/journal.ppat.1002909
- 9. Everitt AR, Clare S, McDonald JU, Kane L, Harcourt K, Ahras M, et al. Defining the range of pathogens susceptible to Ifitm3 restriction using a knockout mouse model. *PloS One.* (2013) 8:e80723. doi: 10.1371/journal.pone.0080723
- 10. Everitt AR, Clare S, Pertel T, John SP, Wash RS, Smith SE, et al. IFITM3 restricts the morbidity and mortality associated with influenza. *Nature*. (2012) 484:519–23. doi: 10.1038/nature10921
- 11. Zani A, Yount JS. Antiviral protection by IFITM3 in vivo. Curr Clin Microbiol Rep. (2018) 5:229–37. doi: 10.1007/s40588-018-0103-0
- 12. Allen EK, Randolph AG, Bhangale T, Dogra P, Ohlson M, Oshansky CM, et al. SNP-mediated disruption of CTCF binding at the IFITM3 promoter is associated with risk of severe influenza in humans. *Nat Med.* (2017) 23:975–83. doi: 10.1038/nm.4370

#### Generative AI statement

The author(s) declare that no Generative AI was used in the creation of this manuscript.

Any alternative text (alt text) provided alongside figures in this article has been generated by Frontiers with the support of artificial intelligence and reasonable efforts have been made to ensure accuracy, including review by the authors wherever possible. If you identify any issues, please contact us.

#### Publisher's note

All claims expressed in this article are solely those of the authors and do not necessarily represent those of their affiliated organizations, or those of the publisher, the editors and the reviewers. Any product that may be evaluated in this article, or claim that may be made by its manufacturer, is not guaranteed or endorsed by the publisher.

#### Supplementary material

The Supplementary Material for this article can be found online at: https://www.frontiersin.org/articles/10.3389/fimmu.2025.1647166/full#supplementary-material

- 13. Gholami M, Sakhaee F, Sotoodehnejadnematalahi F, Zamani MS, Ahmadi I, Anvari E, et al. Increased risk of COVID-19 mortality rate in IFITM3 rs6598045 G allele carriers infected by SARS-CoV-2 delta variant. *Hum Genomics*. (2022) 16:60. doi: 10.1186/s40246-022-00434-8
- 14. Kim YC, Jeong MJ, Jeong BH. Strong association of regulatory single nucleotide polymorphisms (SNPs) of the IFITM3 gene with influenza H1N1 2009 pandemic virus infection. *Cell Mol Immunol.* (2020) 17:662–4. doi: 10.1038/s41423-019-0322-1
- 15. Schönfelder K, Breuckmann K, Elsner C, Dittmer U, Fistera D, Herbstreit F, et al. The influence of IFITM3 polymorphisms on susceptibility to SARS-CoV-2 infection and severity of COVID-19. *Cytokine*. (2021) 142:155492. doi: 10.1016/j.cyto.2021.155492
- 16. Xuan Y, Wang LN, Li W, Zi HR, Guo Y, Yan WJ, et al. IFITM3 rs12252 T>C polymorphism is associated with the risk of severe influenza: a meta-analysis. *Epidemiol Infect.* (2015) 143:2975–84. doi: 10.1017/S0950268815000278
- 17. Cossart P, Helenius A. Endocytosis of viruses and bacteria. Cold Spring Harb Perspect Biol. (2014) 6:a016972. doi: 10.1101/cshperspect.a016972
- 18. Mercer J, Schelhaas M, Helenius A. Virus entry by endocytosis. *Annu Rev Biochem.* (2010) 79:803–33. doi: 10.1146/annurev-biochem-060208-104626
- 19. Barrow E, Nicola AV, Liu J. Multiscale perspectives of virus entry via endocytosis. *Virol J.* (2013) 10:177. doi: 10.1186/1743-422X-10-177
- 20. Grove J, Marsh M. The cell biology of receptor-mediated virus entry. J Cell Biol. (2011) 195:1071–82. doi: 10.1083/jcb.201108131
- 21. Zhao X, Li J, Winkler CA, An P, Guo JT. IFITM genes, variants, and their roles in the control and pathogenesis of viral infections. *Front Microbiol.* (2018) 9:3228. doi: 10.3389/fmicb.2018.03228
- 22. Ren L, Du S, Xu W, Li T, Wu S, Jin N, et al. Current progress on host antiviral factor IFITMs. Front Immunol. (2020) 11:543444. doi: 10.3389/fimmu.2020.543444
- 23. Shan Z, Han Q, Nie J, Cao X, Chen Z, Yin S, et al. Negative regulation of interferon-induced transmembrane protein 3 by SET7-mediated lysine monomethylation. *J Biol Chem.* (2013) 288:35093–103. doi: 10.1074/jbc.M113.511949
- 24. Chesarino NM, McMichael TM, Hach JC, Yount JS. Phosphorylation of the antiviral protein interferon-inducible transmembrane protein 3 (IFITM3) dually

regulates its endocytosis and ubiquitination. *J Biol Chem.* (2014) 289:11986–92. doi: 10.1074/ibc.M114.557694

- 25. McMichael TM, Zhang L, Chemudupati M, Hach JC, Kenney AD, Hang HC, et al. The palmitoyltransferase ZDHHC20 enhances interferon-induced transmembrane protein 3 (IFITM3) palmitoylation and antiviral activity. *J Biol Chem.* (2017) 292:21517–26. doi: 10.1074/jbc.M117.800482
- 26. Chesarino NM, McMichael TM, Yount JS. Regulation of the trafficking and antiviral activity of IFITM3 by post-translational modifications. *Future Microbiol.* (2014) 9:1151–63. doi: 10.2217/fmb.14.65
- 27. Yount JS, Karssemeijer RA, Hang HC. S-palmitoylation and ubiquitination differentially regulate interferon-induced transmembrane protein 3 (IFITM3)-mediated resistance to influenza virus. *J Biol Chem.* (2012) 287:19631–41. doi: 10.1074/jbc.M112.362095
- 28. Chesarino NM, McMichael TM, Yount JS. E3 ubiquitin ligase NEDD4 promotes influenza virus infection by decreasing levels of the antiviral protein IFITM3. *PloS Pathog.* (2015) 11:e1005095. doi: 10.1371/journal.ppat.1005095
- 29. Shi G, Chiramel AI, Li T, Lai KK, Kenney AD, Zani A, et al. Rapalogs downmodulate intrinsic immunity and promote cell entry of SARS-CoV-2. *J Clin Invest.* (2022) 132:e160766. doi: 10.1172/JCI160766
- 30. Shi G, Ozog S, Torbett BE, Compton AA. mTOR inhibitors lower an intrinsic barrier to virus infection mediated by IFITM3. *Proc Natl Acad Sci U.S.A.* (2018) 115: E10069–78. doi: 10.1073/pnas.1811892115
- 31. Petrillo C, Thorne LG, Unali G, Schiroli G, Giordano AMS, Piras F, et al. Cyclosporine H overcomes innate immune restrictions to improve lentiviral transduction and gene editing in human hematopoietic stem cells. *Cell Stem Cell*. (2018) 23:820–32.e9. doi: 10.1016/j.stem.2018.10.008
- 32. Prikryl D, Marin M, Desai TM, Du Y, Fu H, Melikyan GB. Cyclosporines antagonize the antiviral activity of IFITMProteins by redistributing them toward the golgi apparatus. *Biomolecules*. (2023) 13:937. doi: 10.3390/biom13060937
- 33. Desai TM, Marin M, Chin CR, Savidis G, Brass AL, Melikyan GB. IFITM3 restricts influenza A virus entry by blocking the formation of fusion pores following virus-endosome hemifusion. *PloS Pathog.* (2014) 10:e1004048. doi: 10.1371/journal.ppat.1004048
- 34. Guo X, Steinkühler J, Marin M, Li X, Lu W, Dimova R, et al. Interferon-induced transmembrane protein 3 blocks fusion of diverse enveloped viruses by altering mechanical properties of cell membranes. *ACS Nano*. (2021) 15:8155–70. doi: 10.1021/acsnano.0c10567
- 35. Sood C, Marin M, Chande A, Pizzato M, Melikyan GB. SERINC5 protein inhibits HIV-1 fusion pore formation by promoting functional inactivation of envelope glycoproteins. *J Biol Chem.* (2017) 292:6014–26. doi: 10.1074/jbc.M117.777714
- 36. Hammonds J, Chen X, Zhang X, Lee F, Spearman P. Advances in methods for the production, purification, and characterization of HIV-1 Gag-Env pseudovirion vaccines. *Vaccine*. (2007) 25:8036–48. doi: 10.1016/j.vaccine.2007.09.016
- 37. Miyauchi K, Kim Y, Latinovic O, Morozov V, Melikyan GB. HIV enters cells via endocytosis and dynamin-dependent fusion with endosomes. Cell. (2009) 137:433–44. doi: 10.1016/j.cell.2009.02.046
- 38. Schindelin J, Arganda-Carreras I, Frise E, Kaynig V, Longair M, Pietzsch T, et al. Fiji: an open-source platform for biological-image analysis. *Nat Methods.* (2012) 9:676–82. doi: 10.1038/nmeth.2019
- 39. Bolte S, Cordelières FP. A guided tour into subcellular colocalization analysis in light microscopy. *J Microsc.* (2006) 224:213–32. doi: 10.1111/j.1365-2818.2006.01706.x
- 40. Fan HY, Heerklotz H. Digitonin does not flip across cholesterol-poor membranes. *J Colloid Interface Sci.* (2017) 504:283–93. doi: 10.1016/j.jcis.2017.05.034
- 41. London E, Brown DA. Insolubility of lipids in triton X-100: physical origin and relationship to sphingolipid/cholesterol membrane domains (rafts). *Biochim Biophys Acta.* (2000) 1508:182–95. doi: 10.1016/s0304-4157(00)00007-1
- 42. Spence JS, He R, Hoffmann HH, Das T, Thinon E, Rice CM, et al. IFITM3 directly engages and shuttles incoming virus particles to lysosomes. *Nat Chem Biol.* (2019) 15:259–68. doi: 10.1038/s41589-018-0213-2
- 43. Jia R, Pan Q, Ding S, Rong L, Liu SL, Geng Y, et al. The N-terminal region of IFITM3 modulates its antiviral activity by regulating IFITM3 cellular localization. *J Virol*. (2012) 86:13697–707. doi: 10.1128/JVI.01828-12
- 44. Escola JM, Kleijmeer MJ, Stoorvogel W, Griffith JM, Yoshie O, Geuze HJ. Selective enrichment of tetraspan proteins on the internal vesicles of multivesicular endosomes and on exosomes secreted by human B-lymphocytes. *J Biol Chem.* (1998) 273:20121–7. doi: 10.1074/jbc.273.32.20121
- 45. Kobayashi T, Vischer UM, Rosnoblet C, Lebrand C, Lindsay M, Parton RG, et al. The tetraspanin CD63/lamp3 cycles between endocytic and secretory compartments in human endothelial cells. *Mol Biol Cell*. (2000) 11:1829–43. doi: 10.1091/mbc.11.5.1829
- 46. Kobayashi T, Beuchat MH, Chevallier J, Makino A, Mayran N, Escola JM, et al. Separation and characterization of late endosomal membrane domains. *J Biol Chem.* (2002) 277:32157–64. doi: 10.1074/jbc.M202838200
- 47. Peng T, Hang HC. Site-specific bioorthogonal labeling for fluorescence imaging of intracellular proteins in living cells. *J Am Chem Soc.* (2016) 138:14423–33. doi: 10.1021/jacs.6b08733

- 48. Weston S, Czieso S, White IJ, Smith SE, Kellam P, Marsh M. A membrane topology model for human interferon inducible transmembrane protein 1. *PloS One*. (2014) 9:e104341. doi: 10.1371/journal.pone.0104341
- 49. Bailey CC, Kondur HR, Huang IC, Farzan M. Interferon-induced transmembrane protein 3 is a type II transmembrane protein. *J Biol Chem.* (2013) 288:32184–93. doi: 10.1074/jbc.M113.514356
- 50. Jia R, Xu F, Qian J, Yao Y, Miao C, Zheng YM, et al. Identification of an endocytic signal essential for the antiviral action of IFITM3. *Cell Microbiol.* (2014) 16:1080–93. doi: 10.1111/cmi.12262
- 51. Sun F, Xia Z, Han Y, Gao M, Wang L, Wu Y, et al. Topology, antiviral functional residues and mechanism of IFITM1. *Viruses.* (2020) 12:295. doi: 10.3390/v12030295
- 52. Li K, Jia R, Li M, Zheng YM, Miao C, Yao Y, et al. A sorting signal suppresses IFITM1 restriction of viral entry. *J Biol Chem.* (2015) 290:4248–59. doi: 10.1074/jbc.M114.630780
- 53. Weidner JM, Jiang D, Pan XB, Chang J, Block TM, Guo JT. Interferon-induced cell membrane proteins, IFITM3 and tetherin, inhibit vesicular stomatitis virus infection via distinct mechanisms. J Virol. (2010) 84:12646–57. doi: 10.1128/JVI.01328-10
- 54. Appourchaux R, Delpeuch M, Zhong L, Burlaud-Gaillard J, Tartour K, Savidis G, et al. Functional mapping of regions involved in the negative imprinting of virion particle infectivity and in target cell protection by interferon-induced transmembrane protein 3 against HIV-1. *J Virol.* (2019) 93:e01716-18. doi: 10.1128/JVI.01716-18
- 55. Compton AA, Bruel T, Porrot F, Mallet A, Sachse M, Euvrard M, et al. IFITM proteins incorporated into HIV-1 virions impair viral fusion and spread. *Cell Host Microbe*. (2014) 16:736–47. doi: 10.1016/j.chom.2014.11.001
- 56. Gruenberg J, Stenmark H. The biogenesis of multivesicular endosomes. *Nat Rev Mol Cell Biol.* (2004) 5:317–23. doi: 10.1038/nrm1360
- 57. Piper RC, Katzmann DJ. Biogenesis and function of multivesicular bodies. *Annu Rev Cell Dev Biol.* (2007) 23:519–47. doi: 10.1146/annurev.cellbio.23.090506.123319
- 58. Lill NL, Sever NI. Where EGF receptors transmit their signals. Sci Signal. (2012) 5:e41. doi: 10.1126/scisignal.2003341
- 59. Tomas A, Futter CE, Eden ER. EGF receptor trafficking: consequences for signaling and cancer. *Trends Cell Biol.* (2014) 24:26–34. doi: 10.1016/j.tcb.2013.11.002
- 60. Ushiro H, Cohen S. Identification of phosphotyrosine as a product of epidermal growth factor-activated protein kinase in A-431 cell membranes. *J Biol Chem.* (1980) 255:8363–5. doi: 10.1016/S0021-9258(18)43497-7
- 61. Schreiber AB, Libermann TA, Lax I, Yarden Y, Schlessinger J. Biological role of epidermal growth factor-receptor clustering. Investigation with monoclonal anti-receptor antibodies. *J Biol Chem.* (1983) 258:846–53. doi: 10.1016/S0021-9258(18)33127-2
- 62. Ivanov AI. Pharmacological inhibition of endocytic pathways: is it specific enough to be useful? *Methods Mol Biol.* (2008) 440:15–33. doi: 10.1007/978-1-59745-178-9 2
- 63. Commisso C, Davidson SM, Soydaner-Azeloglu RG, Parker SJ, Kamphorst JJ, Hackett S, et al. Macropinocytosis of protein is an amino acid supply route in Rastransformed cells. *Nature*. (2013) 497:633–7. doi: 10.1038/nature12138
- 64. Macia E, Ehrlich M, Massol R, Boucrot E, Brunner C, Kirchhausen T. Dynasore, a cell-permeable inhibitor of dynamin. *Dev Cell.* (2006) 10:839–50. doi: 10.1016/j.devcel.2006.04.002
- 65. Jovic M, Sharma M, Rahajeng J, Caplan S. The early endosome: a busy sorting station for proteins at the crossroads. *Histol Histopathol.* (2010) 25:99–112. doi: 10.14670/HH-25.99
- 66. Eden ER, White IJ, Futter CE. Down-regulation of epidermal growth factor receptor signalling within multivesicular bodies. *Biochem Soc Trans.* (2009) 37:173–7. doi: 10.1042/BST0370173
- 67. Mamatis JE, Gallardo-Flores CE, Sangwan U, Tooley TH, Walsh T, Colpitts CC. Induction of antiviral gene expression by cyclosporine A, but not inhibition of cyclophilin A or B, contributes to its restriction of human coronavirus 229E infection in a lung epithelial cell line. *Antiviral Res.* (2023) 219:105730. doi: 10.1016/j.antiviral.2023.105730
- 68. Matsuda S, Moriguchi T, Koyasu S, Nishida E. T lymphocyte activation signals for interleukin-2 production involve activation of MKK6-p38 and MKK7-SAPK/JNK signaling pathways sensitive to cyclosporin A. *J Biol Chem.* (1998) 273:12378–82. doi: 10.1074/jbc.273.20.12378
- 69. Sauerhering I, Kupke A, Meier I, Dietzel E, Hoppe J, Gruber AD, et al. Cyclophilin inhibitors restrict Middle East respiratory syndrome coronavirus interferon- $\lambda$  and in mice. *Eur Respir J.* (2020) 56:1901826. doi: 10.1183/13993003.01826-2019
- 70. Zhong L, Song Y, Marziali F, Uzbekov R, Nguyen XN, Journo C, et al. A novel domain within the CIL regulates egress of IFITM3 from the Golgi and reveals a regulatory role of IFITM3 on the secretory pathway. *Life Sci Alliance.* (2022) 5: e202101174. doi: 10.26508/lsa.202101174
- 71. Gruenberg J. Life in the lumen: The multivesicular endosome. *Traffic.* (2020) 21:76–93. doi: 10.1111/tra.12715
- 72. Zhang Y, Liu Y, Liu H, Tang WH. Exosomes: biogenesis, biologic function and clinical potential. *Cell Biosci.* (2019) 9:19. doi: 10.1186/s13578-019-0282-2

- 73. Baietti MF, Zhang Z, Mortier E, Melchior A, Degeest G, Geeraerts A, et al. Syndecan-syntenin-ALIX regulates the biogenesis of exosomes. *Nat Cell Biol.* (2012) 14:677–85. doi: 10.1038/ncb2502
- 74. Giordano C, Gelsomino L, Barone I, Panza S, Augimeri G, Bonofiglio D, et al. Leptin modulates exosome biogenesis in breast cancer cells: an additional mechanism in cell-to-cell communication. *J Clin Med.* (2019) 8:1027. doi: 10.3390/jcm8071027
- 75. Skryabin GO, Komelkov AV, Savelyeva EE, Tchevkina EM. Lipid rafts in exosome biogenesis. *Biochem (Mosc)*. (2020) 85:177–91. doi: 10.1134/S0006297920020054
- 76. Trajkovic K, Hsu C, Chiantia S, Rajendran L, Wenzel D, Wieland F, et al. Ceramide triggers budding of exosome vesicles into multivesicular endosomes. *Science*. (2008) 319:1244–7. doi: 10.1126/science.1153124
- 77. Larios J, Mercier V, Roux A, Gruenberg J. ALIX- and ESCRT-III-dependent sorting of tetraspanins to exosomes. *J Cell Biol.* (2020) 219:e201904113. doi: 10.1083/jcb.201904113
- 78. Klein S, Golani G, Lolicato F, Lahr C, Beyer D, Herrmann A, et al. IFITM3 blocks influenza virus entry by sorting lipids and stabilizing hemifusion. *Cell Host Microbe*. (2023) 31:616–33.e20. doi: 10.1016/j.chom.2023.03.005
- 79. Amini-Bavil-Olyaee S, Choi YJ, Lee JH, Shi M, Huang IC, Farzan M, et al. The antiviral effector IFITM3 disrupts intracellular cholesterol homeostasis to block viral entry. *Cell Host Microbe*. (2013) 13:452–64. doi: 10.1016/j.chom.2013.03.006
- 80. O'Leary TJ, Levin IW. Raman spectroscopy of selectively deuterated dimyristoylphosphatidylcholine: studies on dimyristoylphosphatidylcholine-cholesterol bilayers. *Biochim Biophys Acta*. (1986) 854:321–4. doi: 10.1016/0005-2736(86)90126-4
- 81. Söderlund T, Lehtonen JY, Kinnunen PK. Interactions of cyclosporin A with phospholipid membranes: effect of cholesterol. *Mol Pharmacol.* (1999) 55:32–8. doi: 10.1124/mol.55.1.32
- 82. Lambros MP, Rahman YE. Effects of cyclosporin A on model lipid membranes. *Chem Phys Lipids*. (2004) 131:63–9. doi: 10.1016/j.chemphyslip.2004.04.002
- 83. Dynarowicz-Łątka P, Wnętrzak A, Makyła-Juzak K. Cyclosporin A in membrane lipids environment: implications for antimalarial activity of the drug-the langmuir monolayer studies. *J Membr Biol.* (2015) 248:1021–32. doi: 10.1007/s00232-015-9814-9

- 84. Das T, Yang X, Lee H, Garst EH, Valencia E, Chandran K, et al. -palmitoylation and Sterol Interactions Mediate Antiviral Specificity of IFITMs. *ACS Chem Biol.* (2022) 17:2109–20. doi: 10.1021/acschembio.2c00176
- 85. Rahman K, Datta SAK, Beaven AH, Jolley AA, Sodt AJ, Compton AA. Cholesterol binds the amphipathic helix of IFITM3 and regulates antiviral activity. *J Mol Biol.* (2022) 434:167759. doi: 10.1016/j.jmb.2022.167759
- 86. Lee J, Robinson ME, Ma N, Artadji D, Ahmed MA, Xiao G, et al. IFITM3 functions as a PIP3 scaffold to amplify PI3K signalling in B cells. *Nature.* (2020) 588:491–7. doi: 10.1038/s41586-020-2884-6
- 87. Unali G, Crivicich G, Pagani I, Abou-Alezz M, Folchini F, Valeri E, et al. Interferon-inducible phospholipids govern IFITM3-dependent endosomal antiviral immunity. *EMBO J.* (2023) 42:e112234. doi: 10.15252/embj.2022112234
- 88. Buchrieser J, Degrelle SA, Couderc T, Nevers Q, Disson O, Manet C, et al. IFITM proteins inhibit placental syncytiotrophoblast formation and promote fetal demise. *Science.* (2019) 365:176–80. doi: 10.1126/science.aaw7733
- 89. Xiong Z, Xu X, Zhang Y, Ma C, Hou C, You Z, et al. IFITM3 promotes glioblastoma stem cell-mediated angiogenesis via regulating JAK/STAT3/bFGF signaling pathway. *Cell Death Dis.* (2024) 15:45. doi: 10.1038/s41419-023-06416-5
- 90. Zani A, Zhang L, McMichael TM, Kenney AD, Chemudupati M, Kwiek JJ, et al. Interferon-induced transmembrane proteins inhibit cell fusion mediated by trophoblast syncytins. *J Biol Chem.* (2019) 294:19844–51. doi: 10.1074/ibc.AC119.010611
- 91. Chu PY, Huang WC, Tung SL, Tsai CY, Chen CJ, Liu YC, et al. IFITM3 promotes Malignant progression, cancer stemness and chemoresistance of gastric cancer by targeting MET/AKT/FOXO3/c-MYC axis. *Cell Biosci.* (2022) 12:124. doi: 10.1186/s13578-022-00858-8
- 92. Perrin P, Janssen L, Janssen H, van den Broek B, Voortman LM, van Elsland D, et al. Retrofusion of intralumenal MVB membranes parallels viral infection and coexists with exosome release. *Curr Biol.* (2021) 31:3884–93.e4. doi: 10.1016/j.cub.2021.06.022